ORNL/TM-2021/1997

Revisions of ORNL ^{188}W Process Based on Nonradiological Experiments

Miting Du
Lance Wyant
Trent Walker
Stephanie Bruffey
Miguel Toro Gonzalez
Stacy Queern
Justin R. Griswold

Approved for public release.
Distribution is unlimited

May 2021

OAK RIDGE National Laboratory

ORNL IS MANAGED BY UT-BATTELLE LLC FOR THE US DEPARTMENT OF ENERGY

ORNL/TM-2021/1997

Radioisotope Science and Technology Division

REVISIONS OF ORNL ^{188}W PROCESS BASED ON NONRADIOLOGICAL EXPERIMENTS

Miting Du
Lance Wyant
Trent Walker
Stephanie Bruffey
Miguel Toro Gonzalez
Stacy Queern
Justin R. Griswold

May 2021

Prepared by
OAK RIDGE NATIONAL LABORATORY
Oak Ridge, TN 37831-6283
managed by
UT-BATTELLE, LLC
for the
US DEPARTMENT OF ENERGY
under contract DE-AC05-00OR22725

CONTENTS

LIST OF FIGURES

LIST OF TABLES

ACRONYMS

DF	dilution factor
DI	deionized
DL	detection limit
HEPA	high efficiency particulate air
HFIR	High Flux Isotope Reactor
ICP-MS	inductively coupled plasma–mass spectrometry
ICP-OES	inductively coupled plasma–optical emission spectroscopy
L/D	length/diameter
MFC	mass flow controller
ORNL	Oak Ridge National Laboratory
ULMF	upper limit of the maximum flow rate
UV-Vis	ultraviolet-visible

ACKNOWLEDGMENTS

This research is supported by the US Department of Energy Isotope Program, managed by the Office of Science.

The authors wish to thank the following colleagues for their strong support of this project:

Carlos R. Flores	Jason Craig
Jenny Conner	Chris Marcus
Julie G. Ezold	Tamara (Tammy) Keever
Leigh R. Martin	Richard Mayes
Paul Benny	Lætitia H. Delmau

ABSTRACT

Tungsten-188 is in widespread use in the $^{188}W(t_{1/2} = 69\ d)/^{188}Re(t_{1/2} = 16.9\ h)$ biomedical generator. Oak Ridge National Laboratory (ORNL) has been providing this product to the world since 1999. At ORNL, ^{188}W is produced via irradiation in ORNL's High Flux Isotope Reactor (HFIR). Enriched ^{186}W targets in the form of sintered metallic pellets or rings achieve a compact loading in the irradiation vessel, providing a high yield per unit target. The enrichment of the target is >90% ^{186}W, and this isotope undergoes double neutron capture to produce the desired ^{188}W product.

Although ^{188}W is produced by neutron bombardment, $^{191}Os(t_{1/2} = 15.4\ d)$ is simultaneously produced as a by-product requiring separation from ^{188}W by post-irradiation treatment. In the current processing pathway, the irradiated W metal pellets or rings are first converted into an oxide form of WO_3 by heating the irradiated W metal target at 750°C in a quartz reaction vessel inside a vertical furnace under a constant flow of air. During heating, W metal reacts with oxygen in the air to produce WO_3, which is soluble in 6 *M* NaOH for later purification process. This oxidation process also converts ^{188}Os (the decay daughter of ^{188}W) and ^{191}Os (the irradiation produced byproduct) into OsO_4, a highly volatile and toxic gas. The gaseous effluents driven from the quartz reaction vessel are passed through a scrubbing array to remove OsO_4 before the air is discharged from the process.

This heterogeneous oxidation method simultaneously achieves two goals: (1) converting metal target to a soluble oxide form and (2) removing volatile OsO_4 away from the solid WO_3 product by air flow and absorbing the harmful Os species by the scrubbing array. In the past 20 years, the existing OsO_4 scrubbing array served well in preventing OsO_4 from being released into the environment; however, in July 2020 a minor amount of ^{191}Os was found to have been released into the environment, which resulted in Building 4501 being put in standby from July 2020 to February 2021.

Since October 20, 2020, a team of researchers from groups of the Radioisotope Science and Technology Division and the Nuclear Energy and Fuel Cycle Division were organized to accomplish the following tasks:

- Fully understand the root causes of the July incident of ^{191}Os release and create a redesigned ^{191}Os scrubbing array to eliminate the possibility of ^{191}Os release during future ^{188}W processing.
- In Phase 1 tests, select an optimal air (O_2) flow rate for the ^{188}W process. The optimal rate will provide sufficient oxygen for oxidation of W metal, while still allowing sufficient residence time for ^{191}Os removal by the scrubbers.
- In Phase 2 tests, confirm the efficiency of the redesigned scrubbing array to absorb excessive amount of nonradiological OsO_4 (generated from Os metal powder) at the selected air flow.
- In Phase 3 tests, simulate the hot cell ^{188}W process by heating pressed nonradiological W–Os pellets in a newly designed quartz vessel and the new array under operation parameters selected in Phase 1 and 2.
- Draft a new operating procedure for processing ^{188}W in hot cells and a report that summarizes the Os mitigation project.

This report summarizes the investigation on root causes from technical aspects in July ^{191}Os release and the corresponding improvement toward the redesigned ^{191}Os scrubbing system. This report presents the efforts made on selecting optimal operational parameters with the new scrubbing array and the newly

designed quartz vessel based on experiment data obtained in Phase 1, 2 and 3 tests. Further revisions for ^{188}W process and additional improvements of W target treatment are also discussed.

1. INTRODUCTION

Tungsten-188 is in widespread use in the $^{188}W(t_{1/2} = 69\ d)/^{188}Re(t_{1/2} = 16.9\ h)$ biomedical generator. Oak Ridge National Laboratory (ORNL) has been providing this product to the world since 1999. Tungsten-188 is produced via irradiation of enriched ^{186}W target at High Flux Isotope Reactor (HFIR) by undergoing a double neutron capture reaction to produce the desired ^{188}W product. Two cycles (~50 days) of irradiation for ^{188}W are required, and the lengthy irradiation produces both Re and Os impurities as well (Figure 1).

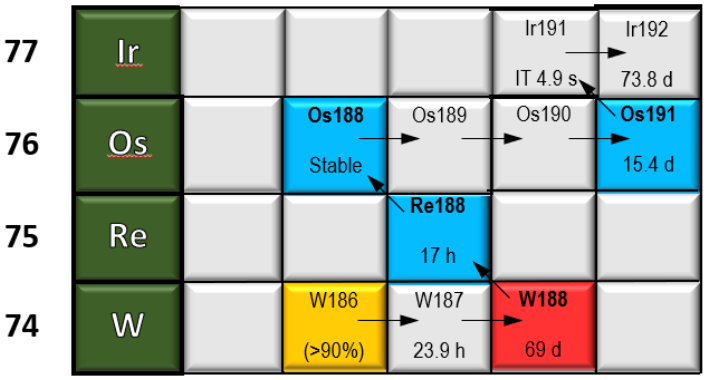

Figure 1. Production pathway for W-188 and its by-products by neutron irradiation.

The pressed and sintered ^{186}W metal rings were chosen as the target form for neutron irradiation because of their high density (19.3 g/cm^3) and high thermal conductivity [0.4 (cal/s)/(cm^3 °C/cm)]. Tungsten's good thermal conductivity is comparable to that of metals such as aluminum (0.5) or copper (0.99). These properties allow for high target loading per target holder (known as *rabbits*), for high target loading per rabbit, increasing the amount of W target per irradiation cycle. The sintered, irradiated targets are not readily dissolved for purification, requiring the conversion of the irradiated W metal target to a soluble oxide form, WO_3, through gas-solid oxidation. The conversion of W to WO_3 has the secondary purpose of separating Os impurities from the ^{188}W product.

1.1 ORNL ^{188}W PROCESS AND ITS INITIAL OsO_4 SCRUBBING SYSTEM

A heterogeneous gas/solid oxidation process was designed in 1999 [1] for one-step conversion of metallic W to WO_3 (Eq. 1) at 750°C for 15 hours in a stream of air (21% O_2), while Re and Os are simultaneously oxidized to semivolatile or volatile oxide forms (Eqs. 2 and 3) and carried out of the heating zone by the air flow (Figure 2), while solid tungsten stays behind in the reaction vessel.

$$2W_{(s)} + 3O_{2(g)} \rightarrow 2WO_{3(s)} \quad (1)$$

$$Os_{(s)} + 2O_{2(g)} \rightarrow OsO_{4(g)} \quad (2)$$

$$2Re_{(s)} + 3O_{2(g)} \rightarrow 2ReO_{3(g)} \qquad 2Re_{(s)} + 7O_{2(g)} \rightarrow 2Re_2O_{7(g)} \quad (3)$$

The toxic and volatile OsO_4 (both ^{191}Os and ^{188}Os) with the air flow is absorbed by a downstream sodium hydroxide (NaOH) scrubber (Eqs. 4 and 5), whereas ReO_3 and Re_2O_7 are sublimed and deposited on top of the quartz reaction vessel outside the heating zone. Noticeably, Eqs. 1–5 are all heterogeneous reactions whose reaction efficiency highly depends on optimal engineering parameter controls.

$$2OsO_{4(g)} + 4NaOH_{(aq)} \rightarrow 2Na_2OsO_{4(aq)} + 2H_2O + O_{2(g)} \quad (4)$$

or $OsO_{4(g)} + 2NaOH_{(aq)} \rightarrow Na_2[OsO_4(OH)_2]_{(aq)}$ (5)

Figure 2 illustrates the equipment that was designed for ^{188}W processing in 1999. The quartz reaction vessel was designed with two concentric quartz tubes joint connected. This allows the air to enter the jacket (via the side port) and be heated before reaching the bottom of the reaction vessel, where it reacts with the tungsten metal and then exit the assembly through the chimney (tube B) into a caustic scrubber containing 10 mL of 1 *M* NaOH. The air flow rate used for this setup was 10-20 mL/min.

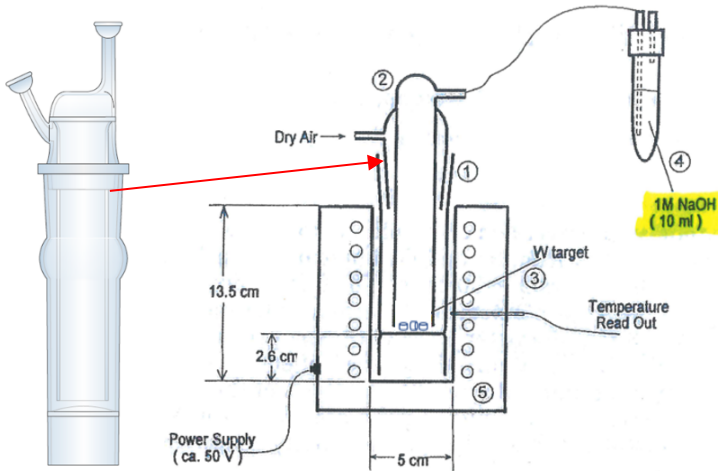

Figure 2. Apparatus for one-step W → WO_3 conversion: (1) tube A, containing W pellets; (2) tube B, where Re deposits on the cooler end; (3) W pellets; (4) NaOH trap for OsO_4; (5) vertical furnace.

In this original design, each load of metallic W comprises three pellets, each 183 mg (96% enriched ^{186}W before irradiation) and being irradiated for 24 days at a neutron flux of 1×10^{15} n.s^{-1}.cm^{-2}. The air flows from a gas cylinder (i.e., positive pressure mode) and is regulated to ~20mL/min for a slow visible flow of gas bubbles shown in the NaOH trap tube. No ^{191}Os release was detected during the initial years of ^{188}W processing in hot cell B of Building 3047.

1.2 CURRENT OsO_4 SCRUBBING ARRAY USED IN CELL A OF BUILDING 4501 SINCE 2006

In 2006, the ^{188}W process was transferred into refurbished Cell A in Building 4501 to increase the scale of production of ^{188}W. The design of the quartz reaction vessel and the vertical furnace were not altered over time, although revisions were made to the OsO_4 scrubbing array (Figure 3). Five key changes were made:

1. The shape of the W metal target was changed from pellets to rings (affording a larger surface area for irradiation and W/WO_3 conversion), and each load of irradiated rings into the quartz vessel increased from the original total 0.55 g to the current total of 4.833 g (as in eight rings). The structure of the quartz vessel was not altered (W metal rings are still on bottom of the vessel).

2. The air flow through the quartz vessel and scrubbing array was changed from positive pressure (supplied by a regulated gas cylinder outside the hot cell) to negative pressure (using cell air pulled into the vessel by a vacuum pump with the air flow regulated by an in-cell rotameter).

3. The original caustic scrubber containing 10 mL of 1 *M* NaOH was modified by increasing the volume to 250 mL and decreasing the concentration of NaOH to 0.1 *M*. The total amount of NaOH was increased from 0.01 to 0.025 mol, corresponding to 2.5 times of increase of available NaOH (vs. 8.8 times increase of the amount of irradiated W metal target).

4. A knockout pot and a charcoal canister were added, with the charcoal bed as a backup solid sorbent for volatile OsO_4. Connections between each stage of the process were made with Tygon tubing, which was found to serve as a deposition surface for OsO_4 as well.

5. The air flow was increased from 20 mL/min to approximately 3–9 L/min as noted in the approved operation procedure [2], and the air flow of 9 L/min became the routine air flow rate for the ^{188}W process in recent years. This is an increase in air flow rate of 450 times.

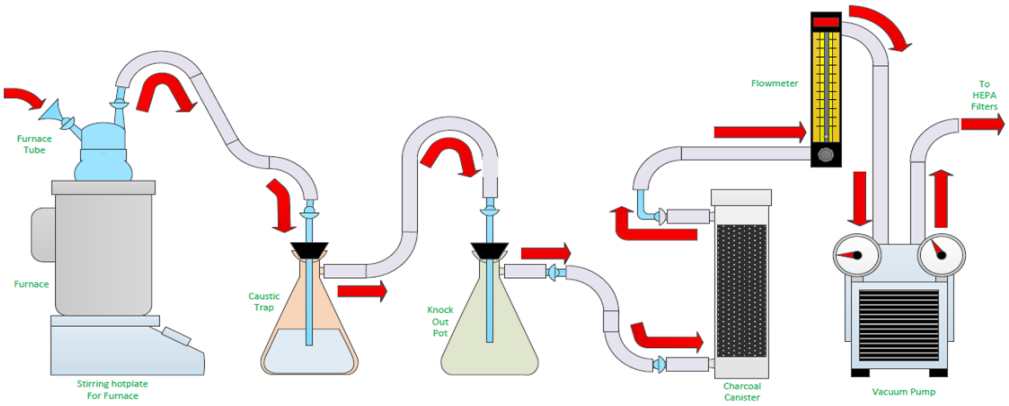

Figure 3. The OsO_4 scrubbing array implemented in ^{188}W process since 2006.

These revisions provided several perceived improvements over the initial scrubbing array, especially the decision to run the air flow using negative pressure. The pressure differential generated by the vacuum pump removed the possibility of gas leakage from these leak-prone joints of the quartz reaction vessel, two rubber stoppers of the knockout pot and the NaOH scrubber. Minor leaks caused through wear and tear of the tubing connections would result in air flow into the system and no OsO_4 would be released into the cell.

The increased W metal load (along with the corresponding increased Os) requires more NaOH to absorb more OsO_4 being generated from the oxidation process. Increasing the amount of NaOH was a step in the right direction, although the 2.5 times increase was not proportional to the 8.8 times increase of the W metal load.

The increased metallic W load requires an increase in the amount of O_2 (air flow reactant). The air flow change from 20 mL/min to approximately 3–9 L/min (450 times of increase) raised the concerns of project members due to the considerable increase of the air flow and its potential effects on the downstream scrubbing operations.

According to Eq. 1, an increase of reactant O_2 would push the reaction forward in terms of thermodynamics. However, the heterogeneous W/O_2 reaction is a slow kinetics reaction controlled by a diffusion process on the metallic W surface. Air flow is an important parameter at lower values, while at higher values increasing the flow rate will not significantly increase the reaction rate. As for the potential effects of the high air flow on the downstream scrubbers, our planned measurements of the upper limit of maximum flow rate (ULMF, an array-specific engineering parameter in scrubber array design) will provide an answer.

The change in system design during the transition from Building 3047 to Building 4501 was advantageous overall. Despite this and several years of successful operation, a OsO_4 release incident

occurred in July 2020. As a result, the project team worked to determine the root cause of the OsO_4 release and provide a safer design for future operation of ^{188}W production process.

To achieve efficient OsO_4 scrubbing (Eqs. 4 and 5), sufficient interaction of gas bubbles with the NaOH solution must occur (the bubbles must travel enough distance, *L*, in NaOH), and sufficient interfacial area of gas bubble and liquid NaOH (enough small sizes of gas bubbles) must be achieved.

The renovations of the OsO_4 scrubbing array were based on above considerations.

1.3 REDESIGNED OsO_4 SCRUBBING ARRAY

The redesigned array that will replace the one currently in Cell A of Building 4501 is shown in Figure 4, with changes listed below.

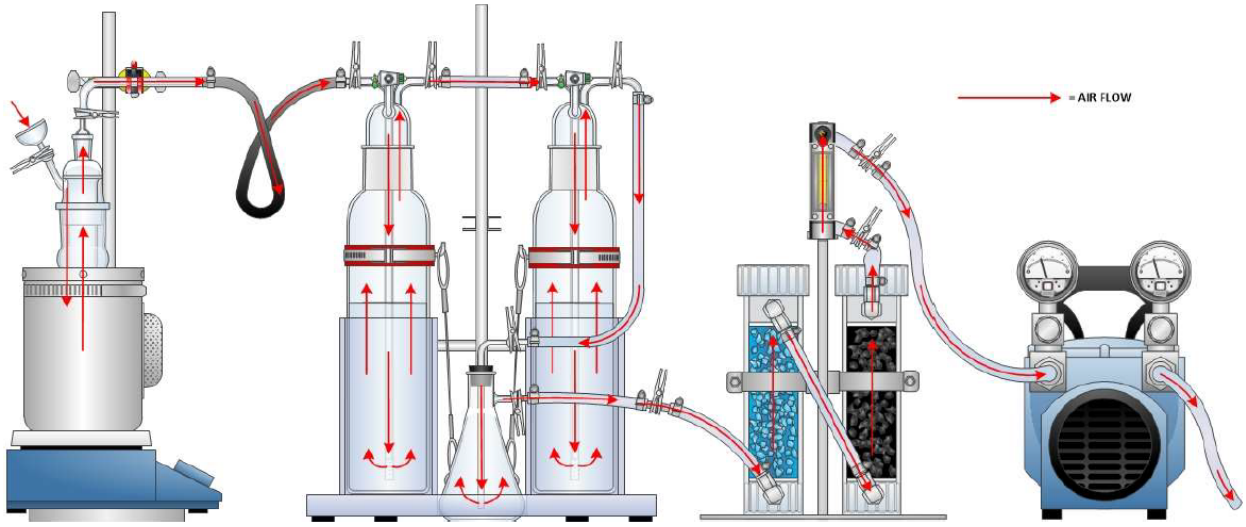

Figure 4. Renovated $^{191}OsO_4$ scrubbing array of new design for ^{188}W process in Building 4501.

1. Added secondary NaOH scrubber for redundancy.

2. Increased the volume of the NaOH to 1.5 L for both the primary and secondary caustic scrubbers.

3. Increased the concentration of NaOH traps from 0.1 *M* to 1 *M* NaOH.

4. Increased the length/diameter (L/D) of NaOH traps to 2.3/1 to increase gas residence time (longer travel distance, ≥18 cm, for gas bubbles in NaOH traps).

5. Added dispersion frits to the inlets of both caustic scrubbers to promote smaller bubble formation and increase the interfacial area of gas bubbles.

In the redesigned array, a vacuum pump pulls ambient cell air into the quartz reaction vessel to oxidize irradiated W metal rings into the WO_3 powder form (at 750°C). The air flow rate is controlled by a rotameter connected to the vacuum pump. During oxidation, semivolatile species (ReO_3 and Re_2O_7) and volatile species (OsO_4) are carried out of the heating zone. The gas is then passed through the two caustic scrubbers in series, a knockout flask, a dryer canister (not used in our tests), and a charcoal canister. Finally, it is discharged into the cell. The cell gas is continuously replaced and undergoes HEPA filtration before being removed from the cell.

Comparing with the current scrubbing array in Building 4501, this new array greatly strengthens OsO_4 absorption capability with liquid sorbent NaOH by increasing number of scrubbers, volume, and concentration of NaOH, L/D of the scrubbers, retention time of gas bubbles in NaOH (small size of gas bubbles and their travel distance in NaOH), and maintains the strong points of 2006 design, such as negative pressure mode, with Tygon tubing/charcoal as supplementary (solid) sorbents for OsO_4. The essential tasks of this project include confirmation of the redesigned scrubbing array effectiveness to prevent any volatile OsO_4 release from this array and to improve the conversion reaction of W → WO_3 and enhance the reaction speed to shorten the reaction time (currently 2–3 days).

1.4 PLANNED EXPERIMENTAL TASKS

No radioactive tests were conducted by this project in a nonradiological laboratory. All nonradiological tasks were conducted in three phases, with tasks in each phase summarized in Table 1. Availability of equipment and materials determined the phase of experiments. For example, furnace and pressed W or W–Os pellets were only available during period of Phase 3 for simulation of OsO_4 generation by a similar heating method as in campaigns.

All nonradiological experiments were performed with the array parameters of the new design, with a few exceptions. (1) scrubbers used had screw-in top lids, which allowed for tests to be operated in either positive pressure (+P) or negative pressure modes (-P), (2) glass tubing (instead of Tygon tubing) was used to connect elements of the array when OsO_4 involved in tests, which allowed for a better mass balance as Os deposits on Tygon tubing; and (3) a digital mass flow controller (MFC) was used instead of a rotameter, since it automatically accounts for changes in temperature and pressure. Finally, no drying canister was used, as it was deemed unnecessary for testing.

The aims of Phase 1 were to determine ULMF for the redesigned array and the simulated current array in Cell A of Building 4501. To determine ULMF, the pretasks included (1). the redesign of the array, (2). the manufacture and procurement of specific equipment for the array, and (3). assembly of the array. The redesigned array and a counterpart of current array were tested across a range of flow rates under alternating positive and negative pressure modes.

Phase 2 was to verify that OsO_4 was effectively scrubbed in the redesigned array with no OsO_4 breakthrough. To support this objective, several key tasks were performed. Tygon tubing connections that were used during campaigns and in Phase 1 tests, were replaced with glass tubing to better ensure full OsO_4 delivery to the caustic scrubbers, as Tygon tubing provides deposition surfaces for OsO_4. Without a furnace, generation of OsO_4 during Phase 2 was performed by aqueous oxidation of Os metal powder, and this method was validated as a subtask within Phase 2. Analytical methodology was developed to support the analysis of trapped Os in caustic media, with pursuit of inductively coupled plasma–optical emission spectroscopy (ICP-OES), inductively coupled plasma–mass spectrometry (ICP-MS), and ultraviolet-visible (UV-Vis) analysis. Other subtasks included an evaluation of the rotameter used during the release event and the determination of what Os levels could be expected in the irradiated W targets.

Phase 3 was to validate the scrubbing methodology with a more realistic source term: Os contained within pressed W metal rings and released through furnace oxidation. A secondary objective was to improve the efficiency of the W oxidation process through a redesign of the quartz reaction vessel. To support this testing, pressed Os–W metal pellets and sintered W metal rings were manufactured. Tests were performed to validate that OsO_4 was fully mitigated in the scrubbing array and that the redesigned quartz reaction vessel improved W oxidation efficiency.

Table 1. Planned aims and tasks in three phases of this project.

Phase no.	Aims	OsO_4	Tasks for experiments
1	Determine the apparent ULMF to arrays and the air flow range for future operations	No OsO_4 involved. Air flow only	—Assemble the redesigned array (Tygon tubing allowed) and a counterpart original array —Set up both positive and negative pressure modes (+P and −P) in the array for testing.
2	Verify no OsO_4 breakthrough from the redesigned array under the testing conditions	With OsO_4 generated by an aqueous method with Os metal powder	—Construct the redesigned array by all glass tubing connections (no Tygon tubing allowed). —Confirm the aqueous method for OsO_4 generation. —Determine what level of excess OsO_4 should be used in testing. —Validate the ICP OES, ICP-MS and/or other methods for Os sample analysis. —Validate control parameters in both +P and −P modes of air flow supply. —Calibrate the rotameter in Cell A of Building 4501 used in past 15 years to determine the potential flow rate used during the release event. —Confirm no OsO_4 break through the redesigned array under the testing conditions.
3	—Confirm no OsO_4 breakthrough the redesigned array under simulated hot cell conditions —Improve W oxidation efficiency	(a) OsO_4 generated by heating pressed W–Os metal pellets (b) No OsO_4 involved. Test W oxidation efficiency by heating sintered W metal rings	—Manufacture of W–Os pellets (not sintered) and sintered natural W metal rings (no Os). —Validate furnace heating method for OsO_4 generation. —Confirm no OsO_4 break through the redesigned array under simulated in cell conditions. —Design a new quartz reaction vessel with renovated internal structure intended to improve W oxidation efficiency —Complete a new operation procedure for ^{188}W process in hot cell and author a TM Report as a summary of the project.

2. EXPERIMENTAL

2.1 REAGENTS AND MATERIALS

Osmium metal powder (841 μm or 20 mesh, 99.95%) was purchased from Sigma-Aldrich, and tungsten metal powder (10 μm, 99.99%) and sodium iodide (99.9%) were purchased from Alfa Aesar by Thermo Fisher Scientific. Sodium (meta) periodate (≥99.0%) and hydrochloric acid (HCl) were purchased from Sigma-Aldrich. Normal paraffin hydrocarbon (NPH) was purchased from Exxon Mobil Chemical Co. Osmium standards for ICP-OES analysis were purchased from the ORNL Chemical Separations Group.

The two glass traps (9.4 cm ID × 35 cm H), as well as connecting glass tubing used for array in Phase 2 and 3, were manufactured by the ORNL Glass Shop. The top seal of the two scrubbers was designed with ace thread with a Teflon plug utilizing a Viton o-ring for a proper seal in tests using both +P and −P modes, which is different from the joint type recommended for future production campaigns (Figure 4). The pressed natural W–Os metal pellets and sintered natural W rings were manufactured by the ORNL Stable Isotopes Group. The eight pressed pellets of W–Os metal powder mixture were 4.9254 g (W 3.9785 g and Os 0.9469 g) in total without sintering treatment. The eight pressed natural W rings, after sintering, were 4.8904 g in total.

2.2 O_SO_4 GENERATION METHODS

For convincing experiment results the method of generating OsO_4 in our tests should be the same as in ^{188}W campaigns by heating W–Os in an air flow (Section 1.1). During Phase 1 and 2 tests, furnace and quartz reaction vessels were not available, so an alternative method of generating OsO_4 was needed to perform Phase 2 test. In addition to the heating (dry) method, several aqueous (wet) methods are discussed in the literature, although most of them are in acidic aqueous media. To avoid any impact from acidic vapor on the evaluation of caustic scrubbers' performance, a wet method of OsO_4 generated from water (neutral media) by reaction of Os metal powder with the oxidant sodium periodate ($NaIO_4$) was chosen in trials for Phase 2 experiment. $NaIO_4$ had only been proved to oxidize RuO_2 into RuO_4, and there was no literature documentation to support its oxidation of Os metal powder. Therefore, the trials of $NaIO_4$ with Os metal powder and confirmation of OsO_4 generation became a subproject in our Phase 2 experiments (Section 3.2.3).

2.3 EQUIPMENT INSTALLED FOR EXPERIMENTS OF THREE PHASES

2.3.1 Positive pressure mode (+P) vs. negative pressure mode (−P) for air supply

In Phase 1 tests, the positive pressure mode (+P) and negative pressure mode (−P) were alternately employed to determine the UMLF specific to redesigned scrubbers and to the scrubber of current design. Glass joint connections (in design of quartz vessel and NaOH traps) could pop open in +P mode; therefore, redesigned glass scrubbers were designed as screw-in top seal to sustain both +P and −P pressure and excluded OsO_4 generator during Phase 1 tests. Unlike the −P mode configuration in Figure 4, the +P configuration is shown in Figure 5 and supplies an air flow with a desired flow rate to either the redesigned scrubbers or the current scrubber design in Cell A of Building 4501.

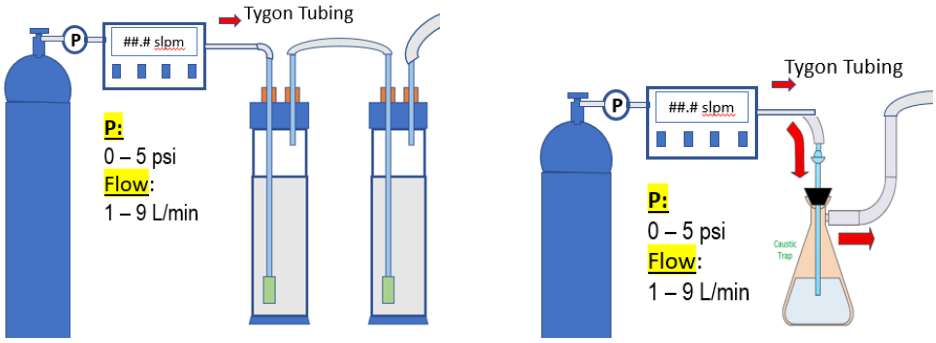

Figure 5. Positive pressure mode to supply air flow into scrubbers in Phase 1 tests.

In Phase 2 of −P mode tests, a three-neck flask for the OsO_4 generator was connected to NaOH traps but with an ambient opening (red arrow in Figure 6) in between. The air flow of 1 L/min, generated by a vacuum pump, was not allowed to pass through the liquid in the OsO_4 generator because of fierce sparging. With an ambient opening, volatile OsO_4 in the generator would not be pulled out of the generator simply by the vacuum pump. Instead, it needed an air flow from gas cylinder to carry the OsO_4 in the generator to join the ambient air in the NaOH trap, so a <70 mL/min air flow was provided by a gas cylinder working in +P mode during the Phase 2 test (Figure 6).

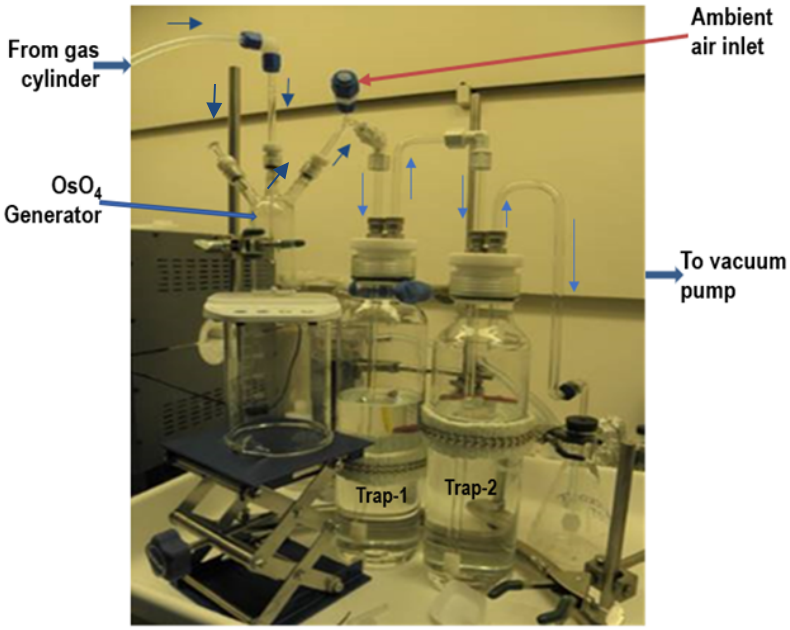

Figure 6. −P mode for 1 L/min air supply with a supplemental +P air flow through OsO_4 generator.

In Phase 3 tests, only −P air flow of 1 L/min obtained using a vacuum pump was pulled through a quartz reaction vessel, NaOH traps, a knockout pot, and a charcoal canister (Figure 4). In both Phase 2 and 3, these array elements were connected by glass tubing instead of Tygon tubing (as in Phase 1) because Tygon tubing is capable of OsO_4 absorption. Glass tubing connections would simplify the Os distribution pattern along the array.

2.3.2 Equipment installed for experiments of three phases

Equipment for experiments of three phases can be categorized as "Air flow mode," "OsO_4 generating," and "Array arrangement" (Table 2).

Table 2. Equipment installed for experiments of three phases.

Phases	Air Flow Mode	OsO_4 Generation	Array Arrangement
1	Tested both +P and −P on current and redesigned arrays with varying rates of air flow from 1 to 9 L/min	Air flow only, with no OsO_4 generator connected	Current array (connected by Tygon tubing): Gas cylinder (flow meter) – Flask with 250 mL deionized (DI) H_2O – knockout – charcoal – off-gas Or Open to ambient air – flask with 250 mL DI H_2O – knockout – charcoal – vacuum pump (MFC) Redesigned array (connected by Tygon tubing): Gas cylinder (flow meter) – 1.5 L NaOH scrubber – 1.5 L NaOH scrubber – knockout – charcoal – off-gas Or Open to ambient air – 1.5 L NaOH scrubber – 1.5 L NaOH scrubber – knockout – charcoal – vacuum pump (with a MFC)
2	Tested by only −P mode at 1 L/min,* with a +P air supply of 50–70 mL/min to push OsO_4 from generator to traps	A three-neck flask for OsO_4 generating by Os + $NaIO_4$ → OsO_4 + I_2 + …	Redesigned array (connected by glass tubing): Gas cylinder (flow meter at 50–70 mL/min) – OsO_4 generator (wet method) – Open ambient air – 1.5 L NaOH scrubber – 1.5 L NaOH scrubber – Knockout – Charcoal – vacuum pump (flow meter at 1 L/min)

Table 2. Equipment installed for experiments of three phases (continued).

Phases	Air Flow Mode	OsO_4 Generation	Array Arrangement
3	Tested by −P mode at 1 L/min only	Heating pressed W–Os metal pellets Heating sintered W rings (No Os)	Redesigned array (connected by glass tubing): Open to ambient air – OsO_4 generator (heating W–Os pellets in quartz vessel) – 1.5 L NaOH scrubber – 1.5 L NaOH scrubber – knockout – charcoal – vacuum pump (MFC at 1 L/min)

* The open ambient air valve (see red arrow in Figure 6) provides air at a rate of 1 L/min pulled by the pump, and the volatile OsO_4 generated in the three-neck flask needs to be pushed out into the scrubbing array by a +P of <70 mL/min air flow. (If directly passing through the generator flask, 1 L/min air flow will result in overflow of the solution inside the three-neck flask).

2.4 EQUIPMENT USED FOR Os SAMPLE ANALYSIS

2.4.1 ICP-OES for Os sample analysis

The Thermo Scientific iCAP 7400 series ICP-OES maintained and operated by the Emerging Isotopes Research Group was used to analyze the Os samples provided in Phase 2 and Phase 3 experiments by this project team. An ICP-OES is an analytical technique to quantify the mass of different elements present in samples. The ICP-OES excites the electrons in the atoms and ions presents using heat energy from the plasma. These electrons emit energy moving from one state to another releasing a photon at a characteristic wavelength. These wavelengths are detected and quantified using Beer–Lambert law to provide the end user with the concentration of the specific element.

Since Os can be absorbed by plastic, minimizing the amount of plastic used in analysis was mandatory. Initially, all sample tubes and pipettes were required to be glass during analysis. However, as analysis progressed, the autosampler was removed to minimize plastic contact with the instrument, and all samples were manually introduced. Although this process is more time-consuming, it minimized the amount of sample needed and the contact time the sample would have with plastic by 40 seconds for each sample. Extra wash time and sample washes were added between samples to further mitigate any carryover of Os from one sample to the next. Further precautions were taken as Os can be volatile when diluted with nitric acid. For this reason, any dilutions were either made with HCl or water.

The ICP-OES standards were made using an analytical grade standard with product certification that provide the stock concentrations. The stock concentrations were used to determine the volume or mass needed to make a dilute set of standards. Typical standard concentrations were 0, 1, 50, 100, 250, 500, and 1,000 ppm with instrument check solutions at 25, 175, and 375 ppm. The appropriate amount of stock solution is aliquoted and diluted with the appropriate solvent, either HCl or water. A typical array of the standards for Os can be seen in Figure 7, and a typical standard calibration curve for the different wavelengths of Os is seen in Figure 8.

Figure 7. Standards and check solutions for Os analysis on the ICP-OES.

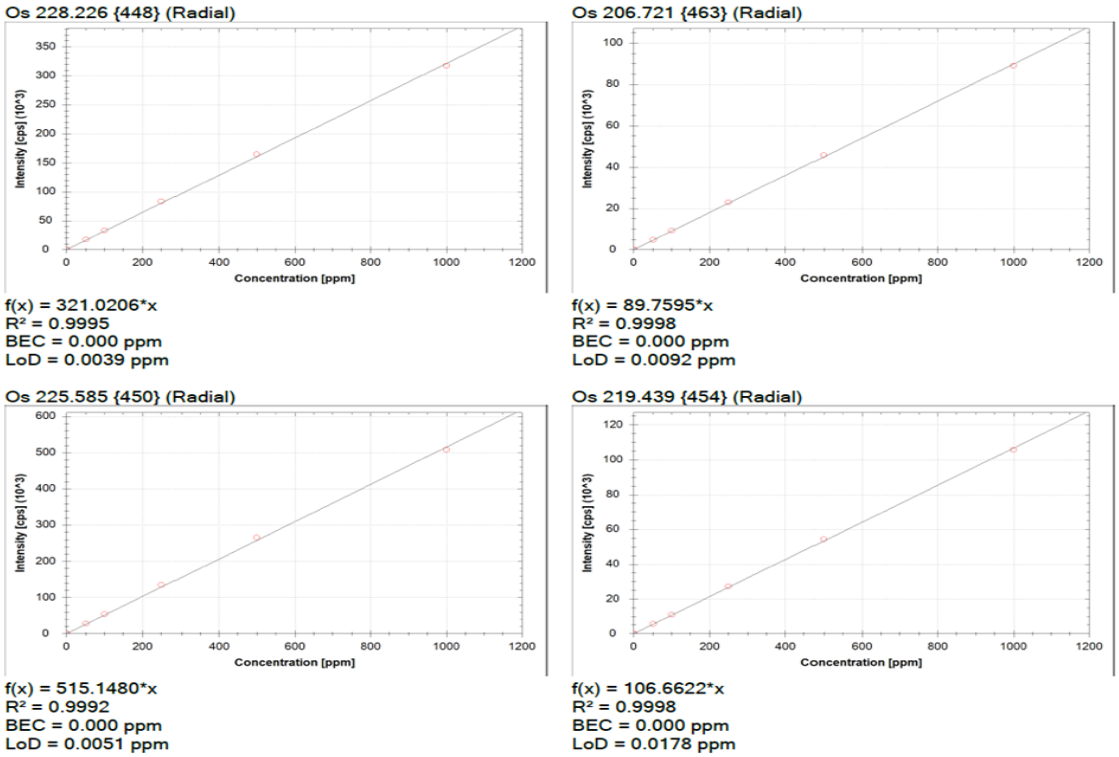

Figure 8. Calibration curves for the Os emissions of 228, 207, 219, and 226 nm.

2.4.2 UV-Vis for Os sample analysis

Ultraviolet-Visible (UV-Vis) spectroscopy was used to analyze Os samples from phase 1 and 2 experiments. UV-Vis is a type of absorption spectroscopy used to characterize and identify different samples based on their absorption of light. UV-Vis can be used to characterize solutions, suspensions, and solids. As a supplement to ICP-OES, UV-Vis can be used to determine the sample concentration based on the Beer–Lambert law.

A Cary 300 UV-Vis spectrophotometer (Agilent technologies) was used to characterize the different samples. This spectrophotometer has a deuterium lamp and is operated using the Cary WinUV Scan application. All samples were analyzed using disposable polystyrene cuvettes with four optical sides and a standard 10 mm path length. A zero correction was applied before recording the absorption spectra between a 200 and 800 nm wavelength range.

UV-Vis spectroscopy demonstrated that an unknown Os species in aqueous NaOH media gives a peak at 370 nm [3]. This was used as a reference to employed UV-Vis spectroscopy in this research, particularly for the comparison of [Os] in different solutions of same NaOH media and similar concentration of iodine species. Therefore, the absorbance (i.e., peak height) at 370 nm was used to determine the presence of Os in the various solutions in Phase 2.

3. RESULTS AND DISCUSSIONS

3.1 PHASE 1 EXPERIMENTS AND DISCOVERY OF ROOT CAUSES OF JULY INCIDENT

Because the factor of 450 increase of the air flow rate (changed from 20 mL/min to 9 L/min) in the design of 2006 became a contentious topic to the project team, our Phase 1 experiments focused on determination of an ULMF to the redesigned scrubbing array and the scrubber of 2006 design (ULMF is an array-specific-parameter). The minimum required air (O_2) in accordance with W metal amount was calculated, as well as the actual air amount used for initial ^{188}W processes.

3.1.1 Minimum required air (O_2) for W/WO_3 and initial 20 mL/min vs. current 9 L/min

Minimum required air (O_2) for specific amount of W metal converting to WO_3 can be calculated by Eq. 1 with an unrealistic assumption of "all O_2 having reacts with W metal"—in reality the air flow provided O_2 will not have chance to fully react with W because reaction of W and O_2 is a heterogeneous reaction that occurs on a W metal surface and is controlled by a diffusion process. Excessive amounts of air are always necessary for a full conversion of W to WO_3. But the calculated minimum can be a good reference to estimate how much air is needed to complete a reaction.

According to Eq. 1, 4.833 g (0.02598 mol, current W load/batch) of W metal requires minimum 5.939 L of air (with 0.03898 mol of O_2 as 21% in air), but 0.55 g (0.002957 mol, W load in 20 years ago) of W requires only 0.676 L of air. In ^{188}W process of initial years, 15 hours of air flow at 20 mL/min satisfied a complete W conversion, with a total 18 L of air consumption, which was 26.6 times of the calculated minimum required air amount for 0.55 g W conversion. Assuming 4.833 g of W takes 15 hours as well (actually 2–3 days during campaigns) for a full conversion at 1 L/min of air flow, the total air consumed would be 900 L, which is >150 times of calculated minimum required air amount for 4.833 g W conversion. Should 9 L/min of air flow be used in the current W → WO_3 process routinely?

One engineering consideration favoring high air flow was that ultrahigh air flow might remove the loose WO_3 powder away from unreacted W metal, which in turn may enhance the W → WO_3 reaction.

The volume change of the solids (from metal rings to loosen WO_3 powder) is obvious (Figure 9), and the powder covers the unreacted W metal surface. Per our practice in later experiments, air flow as high as 7 L/min does not remove the WO_3 powder at all. The structure of the vessel design will not force air to go closer to the unreacted W metal rings on the vessel bottom, but the air will bypass into the chimney in a shortcut way. Meanwhile the ultrahigh air flow may cause unfavorable engineering effects to the follow up ^{191}Os scrubbing system, which was what we were trying to determine during our Phase 1 air flow tests by close observations.

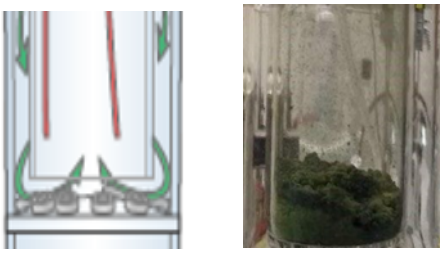

Figure 9. Volume change of the solids in quartz vessel due to W → WO_3.

3.1.2 Gas bubbling behavior and negative engineering effects due to high air flow rate

With equipment arrangement (see Table 2), per −P or +P pressure modes (see Section 2.3.1), both the redesigned array and current Building 4501 array were tested with the air flow at the rate from 1 to 9 L/min. When a counterpart scrubber of current design was assembled with flask/inlet tube of same size and 250 mL liquid, we found that the merged part of air inlet tube in liquid is shorter than 2 cm. Therefore, we tested this scrubber and the scrubber with extended inlet tube for comparison (see Figures 10 and 11). The performance of arrays has been videoed or photographed. Figures 10–12 show gas bubbling in redesigned array or current array (with the inlet tube extended or not) from low to high air flow rates.

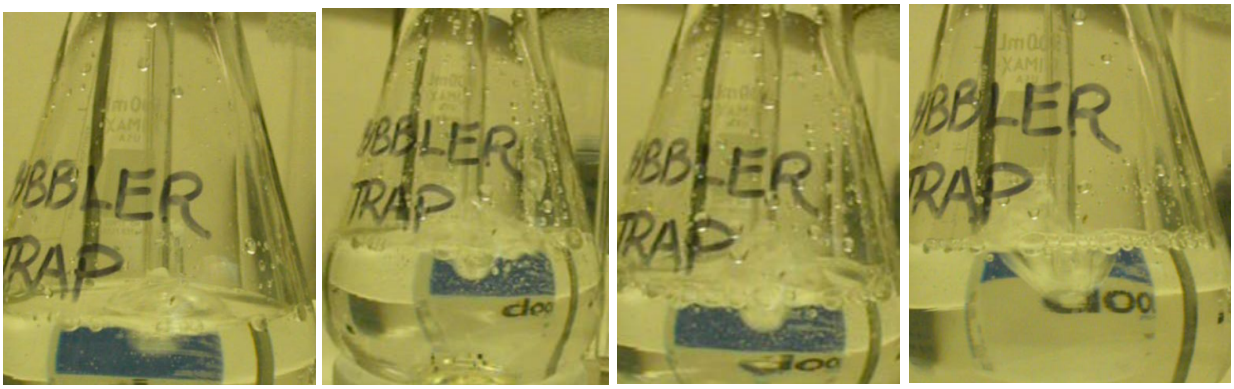

1 L/min **3 L/min** **5 L/min** **7 L/min**

Figure 10. Gas bubbling at different flow rates with current scrubber in Building 4501.

Extending the length of inlet tube by attaching a piece of Tygon tube to the above scrubber, the same round of air flow tests was performed and varied air flow rates in either +P or −P mode:

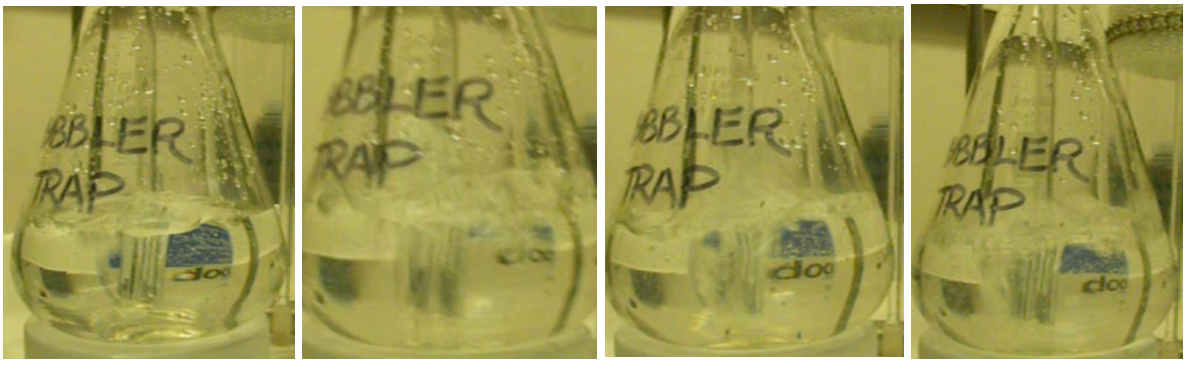

1 L/min **3 L/min** **5 L/min** **7 L/min**

Figure 11. Gas bubbling at different flow rates with the Building 4501 scrubber and extended inlet tube.

Different from the flask shape, redesigned scrubbers are made in column measuring 9.4 cm inner diameter (ID) by 40 cm high with a fine frit air inlet tube (the frit is the part of inlet tube submerged in 1.5 L of 1 *M* NaOH and is >18 cm). With two stages of scrubbers at either −P or +P mode, the air flow tests were performed by varying air flow rates.

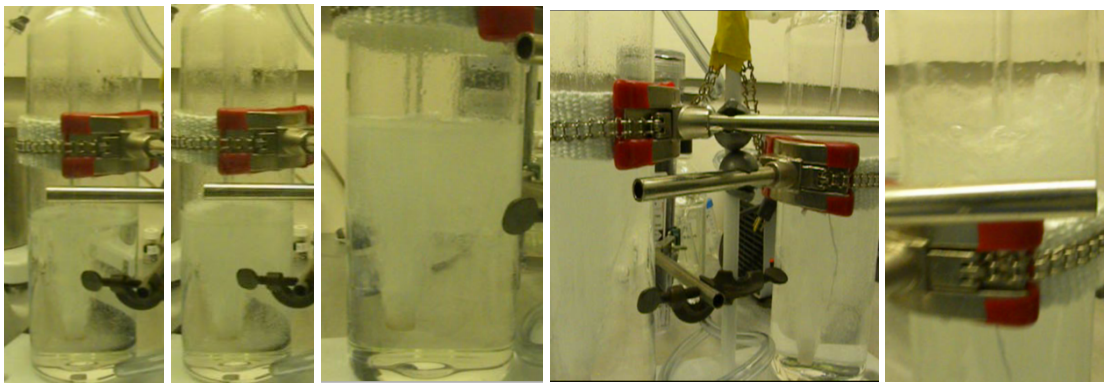

Figure 12. Gas bubbling at different flow rates with redesigned scrubbers.

Interaction of air (OsO_4) and liquid NaOH is a typical heterogeneous reaction between gaseous reactant and the liquid sorbent. For effective and efficient gas/liquid reaction, two engineering parameters are decisive: (1) the size of gas bubbles, and (2) travel distance (*L*) of the gas bubbles. The smaller size of gas bubbles (i.e., larger surface area of bubbles) and the longer distance of bubbles travel through the liquid sorbent (i.e., longer residence time of bubbles in NaOH), the more efficient the interaction of gas bubbles is with the liquid sorbent.

The current scrubber design has a straight open gas inlet tube, which produces large gas bubbles even at slow air flow rates. The part of inlet tube merged in NaOH is only a bit longer than 1 cm (a bit longer than 2 cm after attaching a piece of Tygon tubing), which determines the travel distance (*L*) of the gas bubbles are too short (short residence time) for an interaction of bubbles with the liquid NaOH.

The interaction between a large gas bubble of 150 mL/s (i.e., 9 L/min) with 250 mL of liquid sorbent along a travel distance less than 2 cm is very inefficient. Figures 10 and 11 show that even at 1 L/min air flow a hollow air cavity is formed between the air inlet tube and the liquid surface as the volatile OsO_4 bypasses the liquid scrubber. Figure 13 describes how these two factors influence the OsO_4 scrubbing.

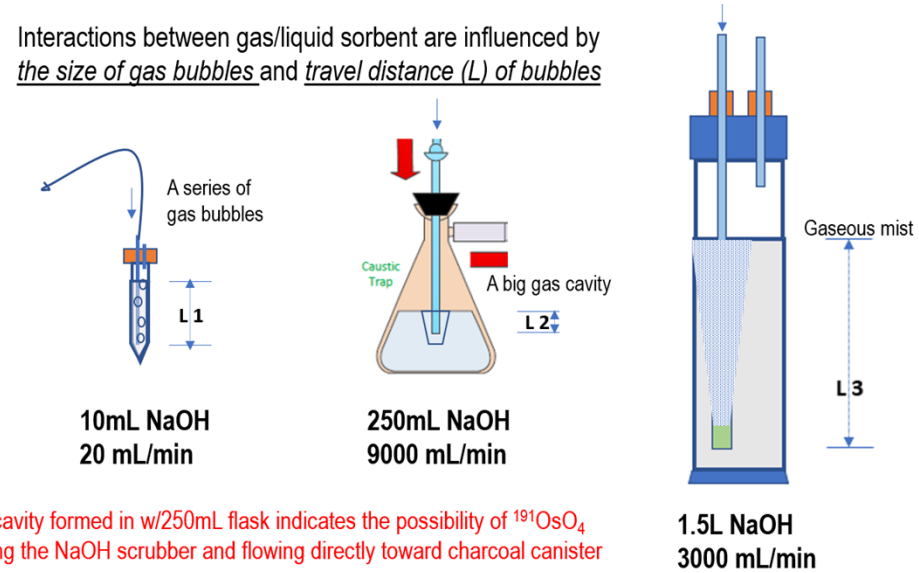

Figure 13. Comparison of three scrubbers explains why 250 mL NaOH does not produce OsO_4 absorption.

Even with the redesigned scrubbing array, obvious gas-liquid turbulence was observed at an air flow of >3 L/min, which may reduce OsO_4 scrubbing efficiency due to OsO_4 carryover.

Therefore, the ULMF of the redesigned scrubbing array is 2 L/min, and the parameters of the array include two stages of 1.5 L 1 *M* NaOH scrubbers with gas inlet tubes (with a fine frit) submerged in NaOH ≥18 cm.

3.1.3 Possible damage to the Tygon tube connected to quartz vessel by heat due to high air flow

Up to now the ultrahigh air flow of 9 L/min has not been found to enhance W → WO_3 reaction but was found as a root cause of the invalid NaOH scrubber in past ^{188}W campaigns (Figure 13).

Another negative consequence of ultrahigh air flow was later discovered during the Phase 3 dry run with the furnace and quartz vessel. Campaign operators confirmed that Tygon tubing was connected to the quartz vessel 2 in. above the glass ball joint on top of the vessel (Figure 3). High air flow brings heat upward. In the Phase 3 dry run, the glass tubing 9 in. above the ball joint reached 140°C at an air flow of 7 L/min and furnace temperature of 750°C. We then specifically measured the temperature 2 in. away from the ball joint at furnace temperature of 750°C, which showed 243°C after 15 min when air flow reached 7 L/min (Figure 14). Remember that 750°C of furnace temperature at 9 L/min in ^{188}W campaigns at Building 4501 would last 2–3 days. The Tygon tubing, connected 2 in. above the glass ball joint, only had a manufacturer defined working temperature of 83°C. The 243°C (or higher) at Tygon tubing connection spot could have caused malfunction of the Tygon tubing in previous campaigns and might have contributed to the July ^{191}Os release incident. The ultrahigh air flow could have caused the high temperature at that spot. At 1 L/min air flow, that spot showed only 40°C with furnace at 750°C.

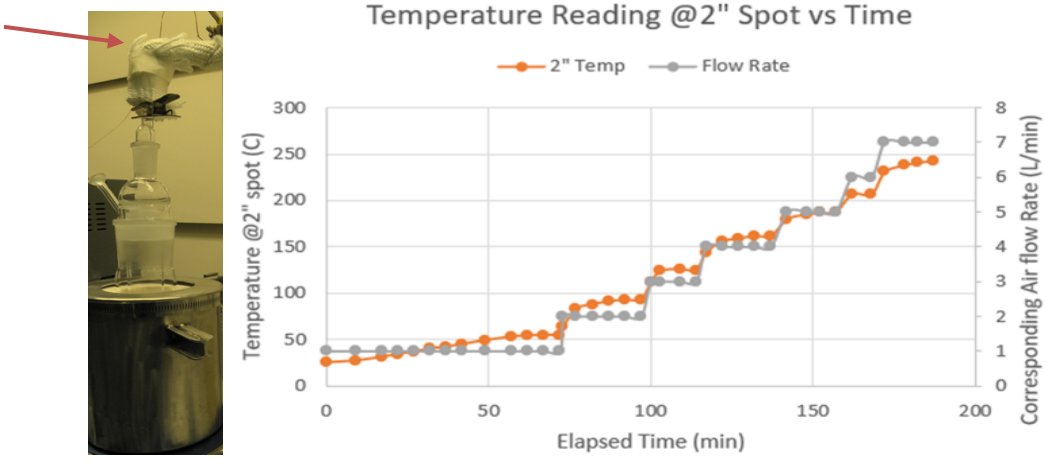

Figure 14. High air flow influence at 2 in. above a ball joint at the top of the furnace at 750°C.

In new equipment assembly, a longer glass tube above the glass ball joint of the quartz vessel was installed for the Viton tubing connection (Figure 4), and the specification for this Viton tubing (instead of Tygon tubing) has a higher working temperature of 280°C.

3.2 PHASE 2 EXPERIMENTS AND REDESIGNED ARRAY PERFORMANCE

The major goal of Phase 2 experiments was to prove that the new scrubbing array will effectively absorb OsO_4 generated during W → WO_3 process. During the period the furnace and quartz vessel were unavailable, we needed to find out a new way to generate OsO_4 from available Os metal powder and pass "enough" OsO_4 into new scrubbers with an Os distribution pattern along the scrubbing array at the

selected air flow rate. Therefore, several tasks were completed to prepare for passing OsO_4 into new scrubbing array and determining the Os distribution pattern.

3.2.1 Glass tubing connections of the array elements and calibration of the rotameter in Building 4501

When examining OsO_4 distribution along the scrubbing array, we want Os being deposited only in traps and not along the tubing. Analysis of samples from two traps and the OsO_4 generator will simplify the assessment of the scrubbing performance. Therefore, all connections between the furnace and scrubbing elements are made of glass because glass tubing has minimal OsO_4 deposits. Glass tubing connections for all elements means a fixture of all equipment and scrubbers by grouping, which is good for simplifying Os distribution measurements during tests but not for campaign operations. Figure 6 shows the glass tubing connected elements in the Phase 2 tests. A vacuum pump (outside Figure 6) is regulated by an MFC and pulling ambient air through an open valve between OsO_4 generator and the first NaOH trap. The air travels into first NaOH trap, second NaOH trap, knockout flask, and a charcoal canister, then out of the off gas of the pump. The valve is kept on instead of off, because controlled 1 L/min air flow is too high to allow entering the three-neck-flask to purge the liquid in flask for OsO_4 being carried out of the flask into the traps. Once the valve is open, the OsO_4 generated in the flask requires additional air flow to carry it out into the NaOH traps. It was why a +P air supply of <70 mL/min was given to carry out OsO_4 in Phase 2 experiment.

A calibration of the rotameter in Cell A of Building 4501 was performed because we needed to know what the exact flow rates being regulated by this rotameter that had not been calibrated since 2006. A gas cylinder and a digital flow meter (mass flow controller or MFC) outside the cell was directly connected by a Teflon tubing to the rotameter inside the cell then off-gassed through a DI water scrubber (Figure 15). The results show that the rotameter was off the range: Its indication of 9 L/min was actually only 6.4 L/min, while its 1 L/min indication was 2.7 L/min. It tells us that since 2006 the expected air flow of 9–10 L/min has been <7 L/min, but operators never reached an air flow <2.7 L/min.

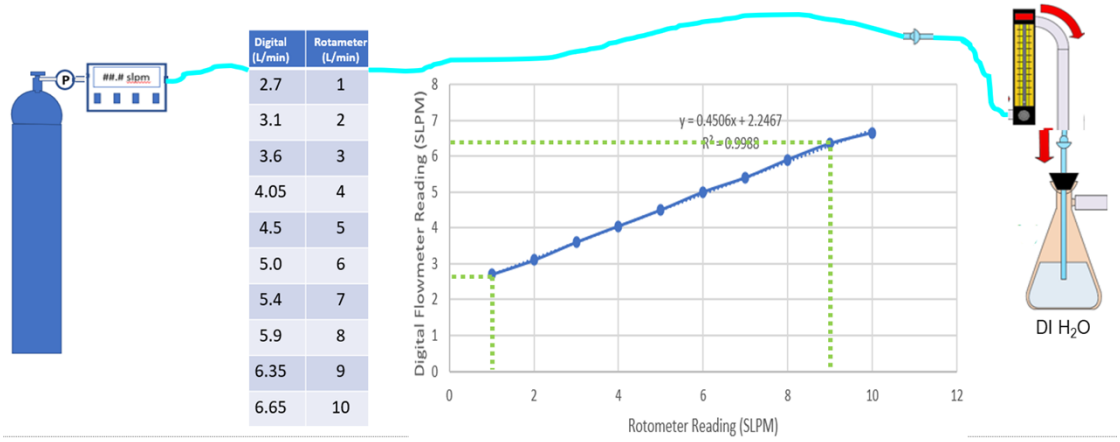

Figure 15. Calibration of the rotameter in Cell A of Building 4501 in +P mold at regulated air flows.

3.2.2 Determination of an input mount of OsO_4 in testing the new scrubbing array

To prove the new scrubbing array is capable of absorbing OsO_4 generated from a fully loaded target with 4.833 g of irradiated W metal, the Phase 2 and 3 demonstrations tested the scrubbing array with more OsO_4 than it is possible to generate with the currently approved target configuration. What is the "most

conservative maximum amount of Os" would be generated after two cycles of neutron irradiation at HFIR at ORNL?

Five different methods [3] were used to determine ^{191}Os yield in July 2020 ^{188}W production campaign. Because of the cycle length and number of days between cycles, the July 2020 campaign is a conservative case for ^{191}Os generation for the two-cycle irradiation of W metal rings. As shown in Ref. [4] and Figure 16, the ISOCHAIN (default) method is the most conservative of the five methods and calculates a yield at the end of bombardment of 175 mCi of ^{191}Os per gram of irradiated W metal.

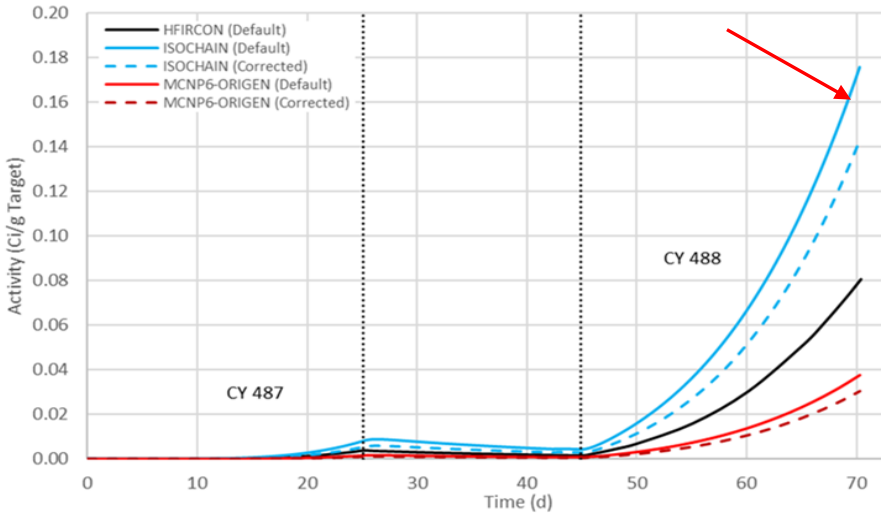

Figure 16. Osmium-191 yield calculations per different models by two cycles of irradiation at HFIR.

Although ^{191}Os decays with a 15.4-day half-life after the second cycle and decreases accordingly, the total Os mass increases because of the decay of radioactive Re and W isotopes to stable Os isotopes. As shown in Figure 17, the maximum Os mass calculated by the ISOCHAIN (default) method plateaus at about 576 mg of Os at 100 days postirradiation for a fully loaded W ring target (normally 40 days cooling).

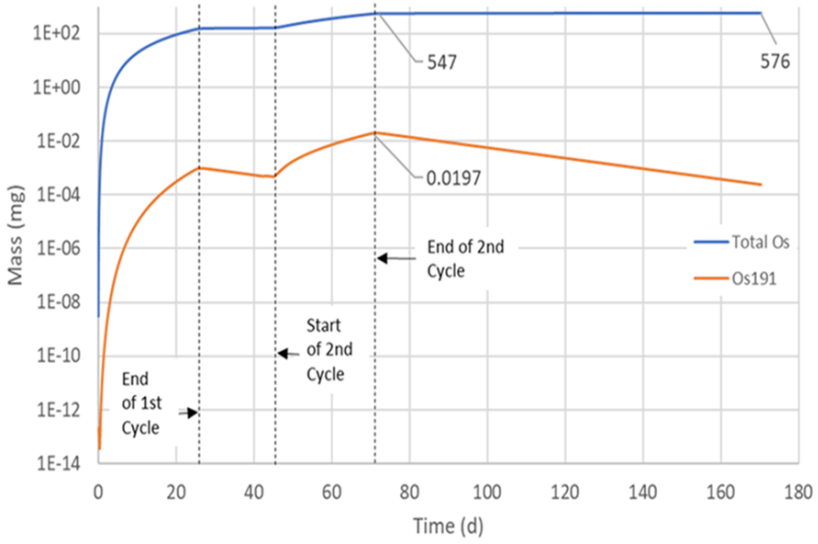

Figure 17. Maximum Os amounts in 4.833 g of irradiated W metal target with cooling days.

Based on the data presented above, we chose to convert 1 g of Os metal into OsO_4. This is almost twice as much Os (if 100% converted to OsO_4) than the most conservative calculation method estimates will be generated in a fully loaded 4.833 g W metal target.

3.2.3 Method confirmation of OsO_4 generating by reacting Os metal with $NaIO_4$ in H_2O

As mentioned in Section 2.2, an aqueous method of generating OsO_4 was needed for Phase 2 test. The literature describes a quick, low-temperature pathway for the generation of RuO_4 [4]. This method oxidizes refractory RuO_2 to volatile RuO_4 in water with $NaIO_4$ as the oxidant. The specific reaction by-products are not known, but a single proposed reaction is shown in Eq. 6 for illustration purposes.

$$RuO_{2(s)} + 2NaIO_{4(aq)} \rightarrow RuO_{4(g)} + 2Na^{+}_{(aq)} + I_{2(g)} + 6OH^{-} + 6H^{+} \quad (6)$$

OsO_2 was not available to the experiment. Will $NaIO_4$ be able to oxidize Os (instead of OsO_2) into desired OsO_4? Thermodynamic calculations using HSC Chemistry indicated that similar reactions could be favorable for the production of OsO_4 from Os metal.

$$7Os_{(s)} + 8NaIO_{4(aq)} \rightarrow 7OsO_{4(g)} + 4I_{2(g)} + 8Na^{+} + 12OH^{-} + 4H^{+} \ (\Delta G = -87.7 \text{ kcal @ } 25°C) \quad (7)$$

To confirm reactivity of $NaIO_4$ with solid Os metal powder, a reaction vessel connected with a 15 mL NaOH trap was built as in Figure 18. The three-neck reaction vessel contained 20 mL of DI water with known amounts of solid Os metal powder with $NaIO_4$ being added into the vessel with stirring at ambient temperature. An air flow of <0.2 L/min was guided into the vessel for sparging and to carry the atmosphere over from the vessel into the connected NaOH trap. Under above experimental conditions, the color of NaOH trap changed from transparent to dark orange within 30 min, and the solid Os metal disappeared in the reaction vessel. Figure 18 shows the color changes of both solutions in the trap and in the reactor within 30 min.

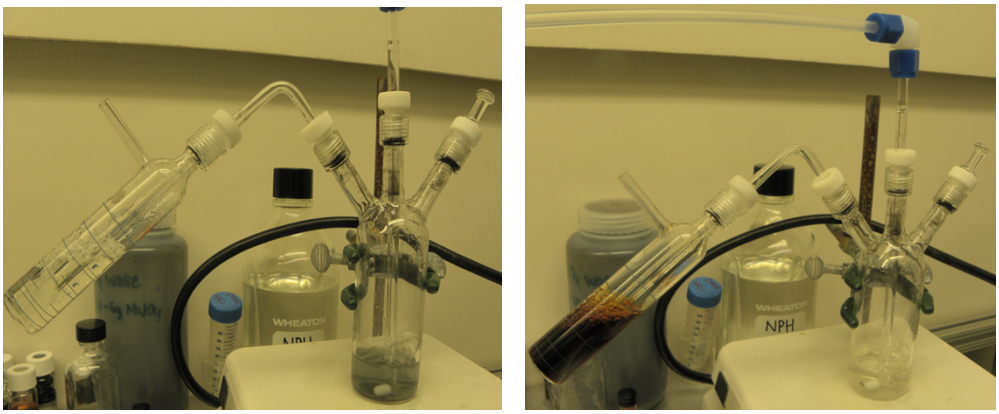

(a) Reaction starts (b) End of reaction: Os(I) species in NaOH trap

Figure 18. Reactivity of $NaIO_4$ with solid Os metal in H_2O: reaction start and end.

When all of the Os metal powder disappeared in the reaction vessel, we realized that the dark orange color in NaOH represented the products (I species and Os species) of the reaction of ($NaIO_4$ + Os), although we were uncertain the chemical speciation of Os being carried from vessel by air flow was in the form of OsO_4 or not.

Experience with the ^{106}Ru recovery projects [6] indicates that the organic diluent, n-paraffin hydrocarbon (NPH), reacts only with RuO_4 (or OsO_4) to form and trap solid RuO_2 (or OsO_2) into the NPH. An experiment specifically to confirm OsO_4 generation was carried out as shown in Figure 19.

DI water and NPH were added into a glass vial to form an aqueous/organic system with a gentle magnetic stirring within aqueous phase. After the Os metal powder and $NaIO_4$ were added into the vial, a cloud of solid OsO_2 grew within the top NPH phase with time (Figure 19[a–c]). As in ^{106}Ru recovery work [6], the solid Os dioxide accumulated in NPH can be back extracted into HCl, after the depleted aqueous phase was replaced with concentrated HCl (Figure 19[d–f]). Because we knew that only tetroxide, as the product from the reaction of (Os + $NaIO_4$), would give the results shown in Figure 19, we were confident in this aqueous method of generating OsO_4 for use in Phase 2 testing.

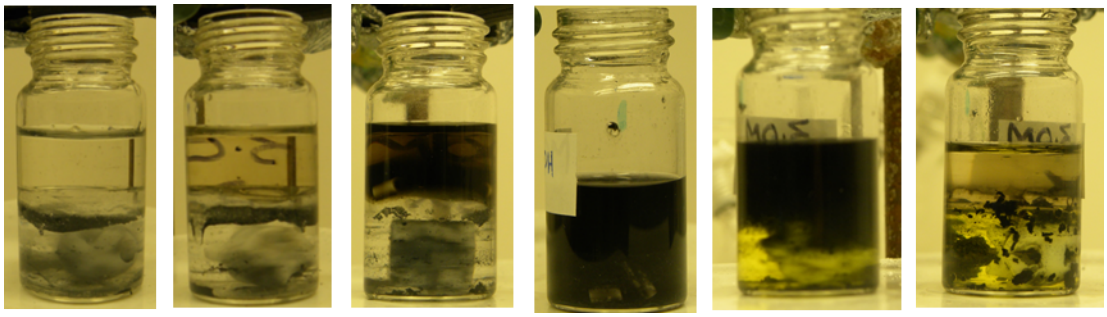

a b c d e f

Figure 19. Solid OsO_2 formation in NPH confirms OsO_4 formation by Os metal + $NaIO_4$.

3.2.4 Phase 2 experiment results, with both OsO_4 and iodine species into scrubbing array

Based on above confirmative experiments we postulate OsO_4 formed by the reaction of $NaIO_4$ with Os metal powder. Because the Os powder disappeared in the reaction vessel and left a clear solution, we assumed the reaction of Os metal was complete, although we do not know how much of reacted Os was converted into OsO_4 (i.e., we have no confirmation of the Eq. 7). We do know that Os metal can be oxidized into OsO_4 (completely or partially) by $NaIO_4$ and enter the NaOH trap with volatile I species (typically as I_2), while iodine species are major contributors to the color of dark orange. Since I_2 and OsO_4 absorption by NaOH are synchronous processes, the orange color of iodine species served as a good indicator for where the Os was located. The volatile iodine species were expected to occupy NaOH's absorbing capacity when using this aqueous method of OsO_4 generating. However, we did not anticipate that the high concentration of I species in Os samples would greatly interfere the analysis of Os content in samples.

The Phase 2 experiment was conducted with the aqueous OsO_4 generator and the scrubbing array displayed in Figure 6. The vacuum pump was turned on and regulated the air flow to 1 L/min from the open valve between the OsO_4 generator (three-neck flask) and the first trap, through the traps, knockout flask, charcoal canister, then the pump off-gas. After the air flow rate stabilized at 1 L/min, 20 mL of DI water was added into the three-neck flask with magnetic stirring, followed by an addition of 1.0059 g of Os metal powder (20 mesh) and 6.0434 g of $NaIO_4$. Air flow of <70 mL/min was guided into the generator flask via an inlet tube from the central port, which resulted in additional sparging of the solution inside the generator to enhance the atmosphere being carried out by +P air flow (this +P air flow was needed to push the volatile OsO_4/iodine species out of the generator into the subsequent NaOH traps.

Volatile OsO_4 and iodine species were generated in the flask by reaction of Os metal and $NaIO_4$, carried over with air flow of 1 L/min into the redesigned scrubbing array. As OsO_4 and iodine species absorbed

by NaOH, the color change of the NaOH scrubber from clear to dark orange (Figure 20) showed a typical color of iodine species in NaOH. Meanwhile, majority of the Os metal powder had dissolved, and the color of solution in generator changed from dark to light with time (Figure 21). To speed up the OsO_4 formation, 3 × 10 mL of DI water was added into the generator flask in batches (resulting volume in flask as 50 mL), and 0.75 g of $NaIO_4$ was added in addition for a total 6.7934 g of $NaIO_4$ in the generator flask, which gave a molar ratio of Os:$NaIO_4$ as 1:6. This ratio is much higher than stoichiometrically required amount of $NaIO_4$ in Eq. 7.

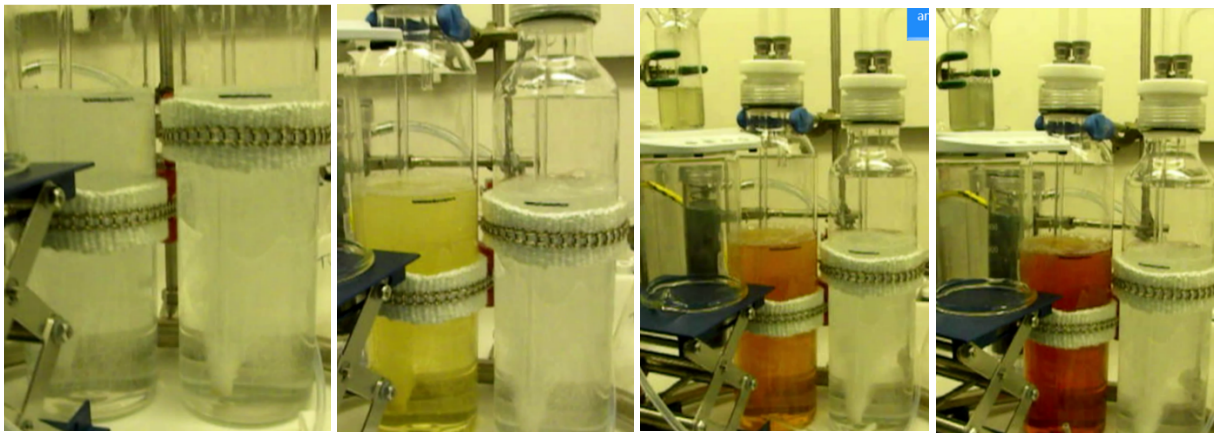

Figure 20. Color changes of NaOH traps in five hours with OsO_4/I being absorbed.

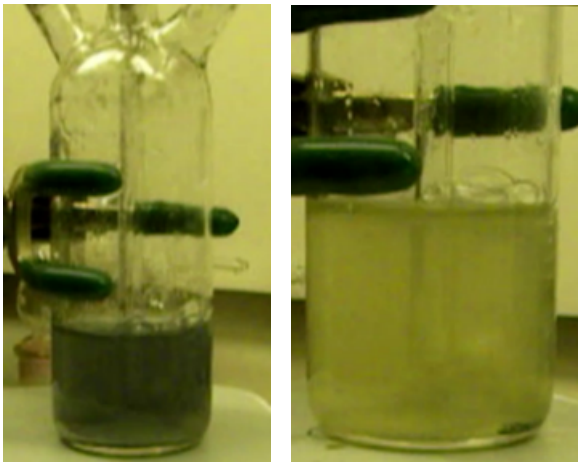

Figure 21. Color change of the solution in OsO_4 generator after OsO_4 is carried away by air flow.

The Phase 2 experiment was stopped after running for 5 hours under the experimental conditions described above, although there were remaining reactants observable inside the OsO_4 generator (Figure 21). Before turning the vacuum pump and the gas cylinder off, a relief valve along the glass tube between the two traps was turned on to allow air into Trap 1. This operation allowed the unbalanced pressure that occurred once the vacuum pump was turned off to neutralize between the two traps.

After the experiment, the 1.5 L NaOH in each trap and 1 *M* NaOH washes of known volume for each trap were split between two 1 L glass bottles for a total of four bottles of solution (Trap 1-1, Trap 1-2, Trap 2-1, and Trap 2-2). Next, the clear supernate was transferred from the generator flask into a glass bottle (G-001) and the remaining solids were rinsed with DI water and stirring before decanting to the bottle of G-001. The final volume of G-001 was 61.5 mL. Concentrated HCl was added dropwise into the generator flask to dissolve the remaining solids, and it was allowed to react overnight. The clear solution (8.2 mL)

was transferred into a glass bottle (G-002). The undissolved solids were air dried and weighed, resulting in a 0.0544 g "undissolved" sample. Formation of crystalline salts on the inside of the glass inlet tube of Trap 1 was observed and later dissolved in DI water pipetted into the tube, which was collected into a glass bottle of "salts in G" (volume: 5.9 mL).

Samples taken from each step were sent for Os content analysis by ICP methods. As a transition metal, multivalent Os presents a versatile speciation in aqueous media at varying acidity or basicity. General spectrometric methods may detect only specific Os species in characterized spectra but not all. Using a high-temperature ICP torch, all Os species in a sample are expected to be atomized into atomic or small polyatomic ions, measured based on mass by a mass spectrometer (ICP-MS) or based on the electromagnetic radiation at wavelengths characteristic of Os by an optical spectrometer (ICP-OES).

There is little in the literature describing Os analysis by either ICP-OES or ICP-MS. Therefore, the Os samples were analyzed by the project team with ICP methods in an attempt to improve available data. Table 3 displays the total Os (mg) amount in each fraction solution based on analysis results in three ICP-OES and two ICP-MS trials. The problem we encountered with the analysis of the samples from Phase 2 test is that sum of subtotals of Os in each fraction are much higher than the carefully weighed original Os metal powder input for the test.

The third round of sample analysis by ICP-OES is used as an example in Table 3:

Table 3. Calculation sheet on the third ICP-OES analysis of samples of Phase 2 test.

1/15/2021	Os (mg)	Tot-V mL	Ave ug/mL	S-mL	226nm	207nm	219nm	228nm
Trap-1	418.368156	1522.5	**274.79025**	5	277.395	277.172	274.59	270.004
Trap-2	0.2850105	1506	**0.18925**	5	0.167	0.285	0.152	0.153
G-001	4141.9532	61.5	**67348.8325**	5	59927.08	72904.4	73466.81	63097.04
G-002	0.33785025	8.2	**41.20125**	5	39.97	42.518	41.621	40.696
Salts in G	11.3431335	5.9	**1922.565**		1894.449	1877.466	1995.78	
Undisslved	0.0544							
sub-total	4572.34175	**4.54552316**	times of input Os					

Three samples were remeasured in the third ICP-OES analysis (OES-3) as highlighted in Table 3, and other sample results in the table were taken from previous runs. As described in Section 2.4.1, averaged Os signals were taken from calibration curves at four emission wavelengths and multiplied with total fraction volume. The results of ICP-OES analysis show the sum of Os amounts in the fractions is still 4.55 times higher than total Os input to the Phase 2 test. (The measured Os amount in G-001 gave >4 times of original Os input to the generator flask.) Table 4 provides a high-level view of the analysis results from the three ICP-OES and two ICP-MS runs.

Table 4. Calculation sheet on fractions of Phase 2 test by ICP-OES/MS analysis.

	Milligrams of Os per Analyzed Results (Input Os total: 1005.9 mg)					
ICP-	*Trap-1*	*Trap-2*	*G-001*	*G-002*	*Salts in G*	*Undissolved*
OES-1	3283.613	44.71916	7254.817	1.39898	11.34313	54.4
OES-2	2318.521	74.14741	3497.253	0.33785		
OES-3	418.3682	0.285011	4141.953			
MS-1	1381.288	66.8242	991.0725			
MS-2	1473.78	93.372	1116.225			
Vol. mL	**1522.5**	**1506**	**61.5**	**8.2**	**5.9**	**Solids**

The fractions of small Os mass from the G-002, salts in G, undissolved, and the Trap 2 samples contributed little to the Os summation. The calculated total Os amounts in either G-001 or Trap 1 (except for OES-3) are multiple times greater the 1.0059 g of Os input for the test, and these two fractions are both mixtures of Os and multiple molar amounts of I species. For this reason, a positive interference in an unknown form from high concentrations of I species became a focus in our troubleshooting.

In the first ICP-OES run, G-001 (highest iodine content) was analyzed as the first in a row of samples, and basic rinses were performed between each sample analysis. In second ICP-OES run, the order of samples remained the same but a few more rinses were performed between each sample analysis. After the "memory effect" was determined to be a major reason for higher analysis results, two adjustments were implemented: the sample analysis order was adjusted, and excessive rinsing was implemented. The sample order was adjusted to analyze the lowest iodine concentration first (Trap 2), moving toward the highest concentration of iodine (G-001), and acid rinses were measured until background was reached. Standard addition was performed to verify matrix interference, but it was found to be lower than 15%. Standards of iodide and Os/iodide mixture were prepared and tested, but no interference was found due to iodide. Samples sent for standard ICP-MS analysis indicated multiple times the Os content than the input Os as well, even though Os standards from two different providers were employed. A hypothesis that would warrant further investigation is the potential formation of a polyatomic ion of Os and I. The Phase 2 analysis shows that similar concentrations of Os and I for sample G-001, which could imply that formation of the polyatomic ion that interferes with the emission wavelengths.

Although we did not achieve a reasonable Os distribution pattern along the scrubbing array because of unknown positive interference within samples with high concentrations of iodine species, we have one concrete conclusion: little Os entered the second NaOH scrubber (see highlighted part of Table 4). With excessive amount of iodine species absorbed in Trap 1, <100 mg of Os (<10% of original Os input) was carried into the Trap 2 scrubber, which gives us the confidence in the OsO_4 scrubbing capability of the new scrubbing array.

3.2.5 UV-Vis analysis of the samples of Os–I from Phase 2 experiment

Although general spectrometric methods (including UV-Vis) may detect only specific Os species in characterized spectra, the literature [5] indicated a specific spectra peak of 370 nm for one of Os species (proposed as in the form of $[Os^{VII}O_3(OH)_3]^{2-}$) in aqueous 2 *M* NaOH. This was used as a reference to employ UV-Vis spectroscopy in this research, particularly for the comparison of [Os] in different solutions of same concentrations of NaOH and similar concentration of iodine species. Therefore, the absorbance (i.e., peak height) at 370 nm was used to determine if the majority of [Os] was found in G-001, T-1, or T-2. Using UV-Vis to calibrate ICP data was performed after Phase 3 data had been obtained but included in Section of 3.2 because of aiming at calibration of Phase 2 sample analysis.

Literature [3] described the 370 nm peak of Os only in a 2 *M* NaOH media. Our experience with UV-Vis analysis of Os samples in NaOH indicated that this specific absorbance, shown at 369 nm by our UV-Vis spectrometer, was within a wide [NaOH] range. The project team researched this absorbance's dependence of [NaOH], [iodine species], and [Os] (370 nm is used in this report to avoid conflicting with the literature).

370 nm absorbance dependence on [NaOH]. An Os–I–2 *M* NaOH solution was obtained in a similar experiment as the one described in Section 3.2.3 and in Figure 18, except using 2 *M* NaOH (instead of using 1 *M* NaOH) as the sorbent for OsO_4 (and iodine species). This 2 *M* NaOH solution contained both OsO_4 and iodine species, and it was prepared in 1, 2, and 3 *M* NaOH samples of the same [Os] and [I] for UV-Vis analysis. The following combinations were used:

Os-I-2M NaOH (mL)	DI H_2O (mL)	NaOH added	[NaOH], resulted
2	0	2mL of 2M	1
2	2	0	2
2	1.58	0.42mL of 50%	3

These three samples were made into different [NaOH] but maintained at the same [Os] and [I], then measured by UV-Vis under the same parameter controls and resulted in comparison of the spectra at 370 nm wavelength absorbance (Figure 22). The dependance of absorbance at 370 nm for the three samples on [NaOH] follows a linear relationship.

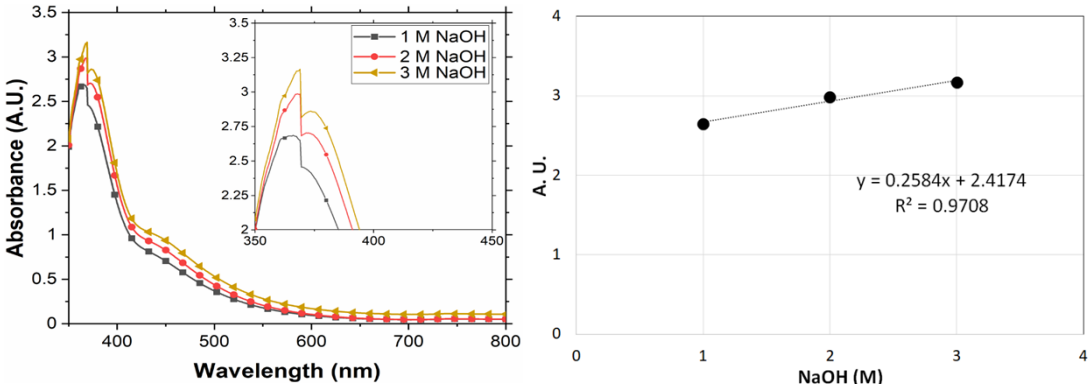

Figure 22. UV-Vis spectra of Os samples at different [NaOH] and a plot of their absorbance at 370 nm vs. [NaOH].

370 nm absorbance dependence on [Os]. Using the above Os–I–2 *M* NaOH with different volumes mixed with 2 *M* NaOH, a set of four 4 mL samples of varying [Os] in 2 *M* NaOH media were made to explore the relationship of absorbance at 370 nm with varying [Os]. The Os content of these four samples was measured by taking the UV-Vis absorbance at a wavelength of 370 nm. A plot of their absorbance at 370 nm vs. dilution factors of [Os] in Figure 23 shows a linear relationship for the Beer–Lambert law validation. Strangely, the absorbance at 370 nm of original Os–I–2 *M* NaOH falls out of the linear regression, and we realized that all these samples were prepared without maintaining [I] at the same level after the knowledge of absorbance dependance on [I] of samples.

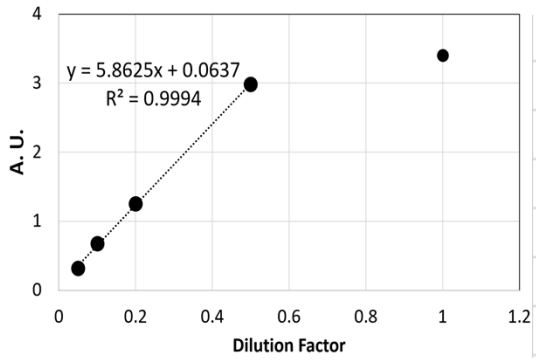

Diluting 2 M NaOH-Os solution with 2 M NaOH

Sample ID	Dilut Times	Os soln mL	2M NaOH mL	Abs (AU)
2M NaOH-Os	1	4	0	3.401999
1	0.5	2	2	2.9858632
2	0.2	0.8	3.2	1.2543551
3	0.1	0.4	3.6	0.6771846
4	0.05	0.2	3.8	0.3204842

Figure 23. A plot of absorbance at 370 nm for samples 1–4 vs. their dilution factors from original.

370 nm absorbance dependence on [iodine]. A sample of 2 *M* NaOH–Os–I was measured by UV-Vis to have a spectrum for comparison, then solid $AgNO_3$ was added into the same UV cuvette (The $AgNO_3$ did not appear dissolved but turned black, which indicates AgI formation.), with an expectation of a slight change of [I] by a reaction of ($Ag^+ + I^- \rightarrow AgI \downarrow$). The solution in the cuvette was measured again using UV-Vis to compare with the measurement taken before the $AgNO_3$ addition.

Figure 24 indicates that the absorbance at 370 nm increases after $AgNO_3$ was added resulting in a decrease of I concentration in same sample solution. Therefore, comparison of 370 nm absorbance of Os species of multiple samples should be done with same [NaOH] and [I] in samples. Because of this knowledge, we realized that the previous Beer–Lambert law validation plotting in Figure 23 was performed with varying concentrations of both Os and I. Figure 23 does show a linear relationship, but the slope/interception of the linear regression should have been influenced by a varying [I] in these samples.

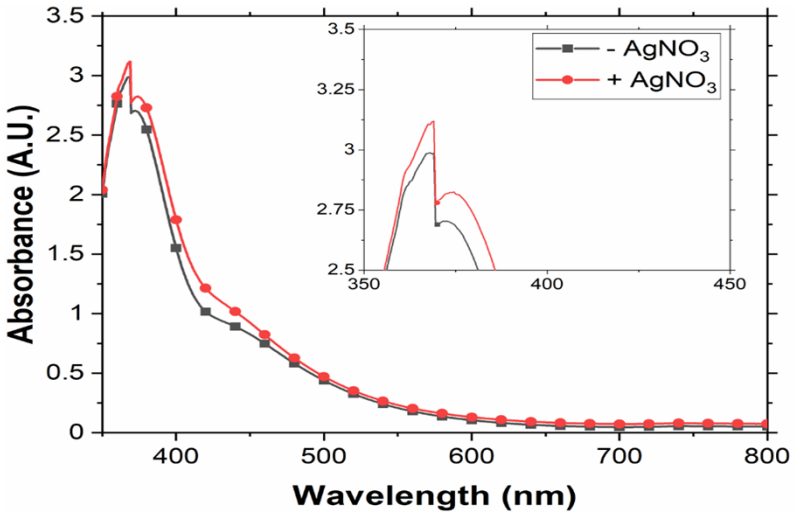

Figure 24. Spectra comparison for the 2 *M* NaOH–Os–I solution before and after the $AgNO_3$ addition.

Comparison of 370 nm absorbance between Trap 1 samples in Phase 2 and 3. Both solutions of Trap 1 in the Phase 2 and Phase 3 experiments (II-T1 and III-T1) were in 1.5 L of 1 *M* NaOH media. II-T1 contains a high concentration of I species, but III-T1 had little iodine contaminant from glass tubing contaminated with residual iodine species. Knowing the ICP data for III-T1 (800 mg Os in 1.5 L NaOH) is reliable compared to II-T1 (418 mg Os in 1.5 L NaOH) by influence of high [I] in II-T1, we prepared one II-T1 sample of the original solution and a series of III-T1 samples of varying dilution times (with 1 *M* NaOH) and measured their absorbance at 370 nm by UV-Vis spectrometry.

In Figure 25, 370 nm absorbance of II-T1 is between that of III-T1 at dilution factor (DF) = 1.2 and 1.3. Per a linear regression of the absorbance at 370 nm for III-T1 samples at DF = 1–2.5, the absorbance at 370 nm of II-T1 (3.190496206) falls into a reflected DF of 1.1772. The ICP-OES result of III-T1 (in Section 3.3) for the total Os in 1.5 L of NaOH solution is 800 mg of Os. With the regressed DF, the reflected total Os in II-T1 solution would be (800/1.1772=) 679.579 mg. Considering the depression of high [I] in II-T1 solution, the absorbance should be >3.1905 if the [I] has no influence. Therefore, efforts with UV-Vis resulted in a different total Os recommendation from the 418 mg Os by the third run of the ICP-OES analysis. Despite of the difference of 680 vs. 418 mg, UV-Vis analysis provided data that supported the second method and negated the first and second ICP-OES results on the Os amount in 1.5 L of the II-T1 solution (3,283 and 2,318 mg).

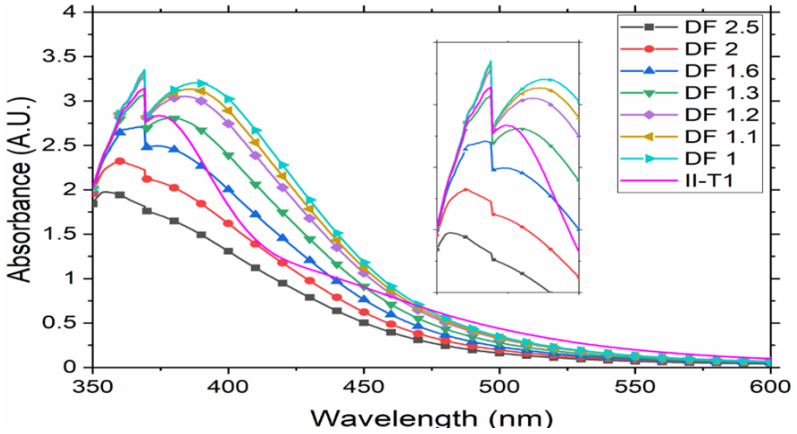

Labels	Vol Orig (mL)	1 M NaOH (mL)	DF	Abs (AU)
II-T1 (1)	**4.0**	**N/A**	**1**	**3.190496206**
III-T1 (1)	4.0	0	1	3.351341009
III-T1(a)	3.75	0.25	1.067	3.322374105
III-T1 (b)	3.5	0.5	1.143	3.283379555
III-T1 (c)	3.0	1.0	1.3	3.075650692
III-T1 (d)	2.5	0.5	1.6	2.698834419
III-T1 (e)	2.0	2	2	2.227408886
III-T1 (f)	1.6	2.4	2.5	1.816929102

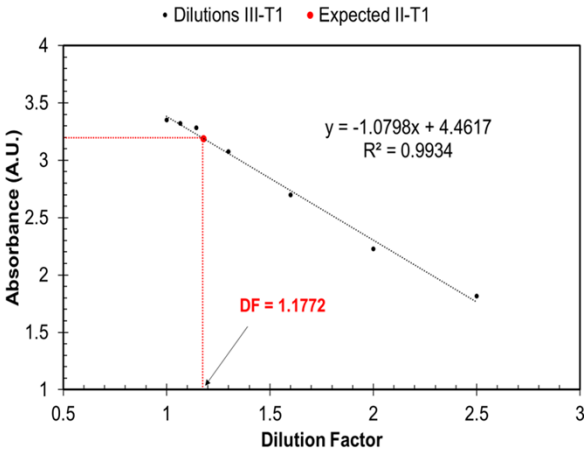

Figure 25. Comparison of 370 nm absorbance in UV-Vis spectra of II-T1 and III-T1 solutions.

Comparison of 370 nm absorbance between III-T1 and II-T1 samples of different dilution. The next task was to compare the UV-Vis spectra of III-T1 (800 mg Os in 1.5 L of 1 *M* NaOH) with that of the II-G1 solution. This is different from spectra comparison of III-T1 and II-T1 (both are in 1 *M* NaOH of same 1.5 L volume) because the original II-G1 solution was in 61.5 mL of DI H_2O media. To compare two solutions using UV-Vis, the original II-G1 needed to be adjusted into the same 1 *M* NaOH as the III-T1 using concentrated NaOH and DI H_2O at the desired ratio; therefore, [Os] of II-G1 samples would be diluted accordingly by the desired DF.

Figure 26 shows spectra of a series of diluted II-G1 samples in 1 *M* NaOH media, as well as a table of four II-G1 samples diluted at different DFs. As for III-T1 sample for UV-Vis analysis, [Os] of the 4 mL

of original 1 *M* NaOH solution would be (800/1500 =) 0.533 mg/mL with no adjustment. Let's assume one of UV-Vis spectra of II-G1 samples diluted by DF = *N*, presents same absorbance (peak height) as that of III-T1 (i.e., 0.533 mg Os/mL), then the total Os in original II-G1 solution can be calculated as (0.533 × N × 61.5 =) 32.78 *N* mg of Os in total 61.5 mL of the original II-G1 sample.

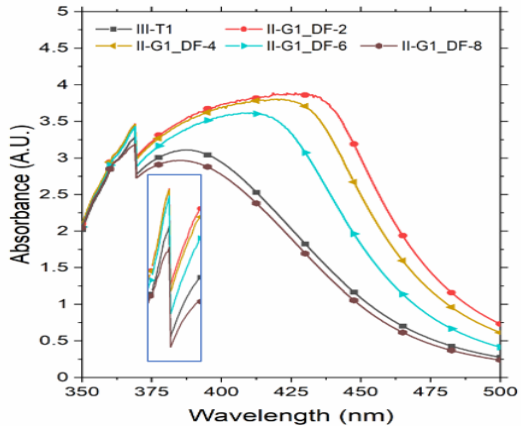

Labels	Vol. of Orig. II-G1	50% NaOH	DI H_2O	D F	Abs (AU)
II-G1_DF-2	2.0 mL	0.21 mL	1.79 mL	2	3.466228
II-G1_ DF-4	1.5 mL	0.21 mL	2.29 mL	2.67	3.461443
II-G1_ DF-6	1.0 mL	0.21 mL	2.89 mL	4	3.431745
II-G1_ DF-8	0.5 mL	0.21 mL	3.29 mL	8	3.192739
Abs (AU) for III-T1 is 3.289915					

Figure 26. Spectra comparison of III-T1 (original) and II-G1 samples of varying DF by UV-Vis.

Figure 26 shows that the absorbance at 370 nm of III-T1 is lower than that of II-G1 samples of DF ≤ 4, but the absorbance is higher than that of II-G1 sample of DF = 8. Ignoring the influence of varying [I] in these II-G1 samples (without I species absorbance at 370 nm would be higher values), the absorbance at 370 nm of II-G1 sample with same value as III-T1 would be DF = 6.4. Therefore, the total Os in 61.5 mL of the original II-G1 solution can be estimated as (0.533 × 6.4 × 61.5 =) 209.79 mg of the total Os in 61.5 mL of the original II-G1 solution.

Using absorbance at 370 nm of III-T1 as a single calibration point, plus the influence by [I], an error range for the estimated Os amount in II-G1 solution should be considered. If using spectrum of DF = 8 as upper limit, the 262 mg Os would be about 1.25 times of the Os obtained at DF= 6.4. We, then, may give the 210 mg Os an error range of ±25% of 210 mg Os.

Per estimated Os amounts in II-T1, II-G1, and II-T2 (provided by ICP analysis), an improved Os distribution pattern along the generator-scrubbers array can be displayed here:

II-G1 (mg)	**II-T1 (mg)**	**II-T2 (mg)**	**Sum of Os in three**	**% of 1.0059 g Os**
210 ± 25%	418 - 680	44.7–93.4	620–1036	62–100%

Although improved by ICP analysis data by efforts on UV-Vis analysis, the Os distribution pattern in Phase 2 along the generator-scrubbing array is not satisfactorily distinct in terms of its error range. But the goal of Phase 2 work was to prove the OsO_4 scrubbing capability of the redesigned scrubbing array (reduced Os breakthrough into Trap 2) using a brand new aqueous method for OsO_4 generation before the furnace and a renovated quartz reaction vessel are available. In addition, all selected control parameters for the redesigned scrubbing system were examined before Phase 3 experiments.

3.3 PHASE 3 EXPERIMENTS AND EFFICIENCY ENHANCEMENT OF W → WO_3

3.3.1 Equipment and material preparation for Phase 3 experiments

Before Phase 3 experiments, a furnace of the same type as in Cell A was prepared for the campaign, and the label of Nationally Recognized Testing Laboratory was renewed.

Eight pressed pellets of a mixture of W metal powder (3.9784 g) and Os metal powder (0.9469 g), as well as eight sintered natural W metal rings (4.8904 g) were manufactured by the Stable Isotopes Group at ORNL (Figure 27). The pressed W–Os metal pellets (6.0 mm outer diameter [OD], average height 1.8 mm), which were not sintered because Os loss in sintering is unwanted (OsO_4 starts forming volatile OsO_4 at 400°C in heating), would be tested in the Phase 3a experiment. The sintered (in 1,400°C for 4 hours) W metal rings (OD 6.13 mm, average height 2.33 mm) would be tested in a Phase 3b experiment.

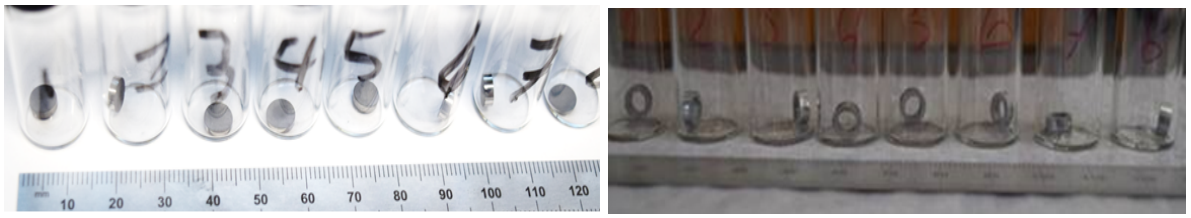

Figure 27. Pressed W–Os metal pellets and sintered natural W metal rings.

The quartz reaction vessel has been revised with new design of its chimney structure (Figure 28).

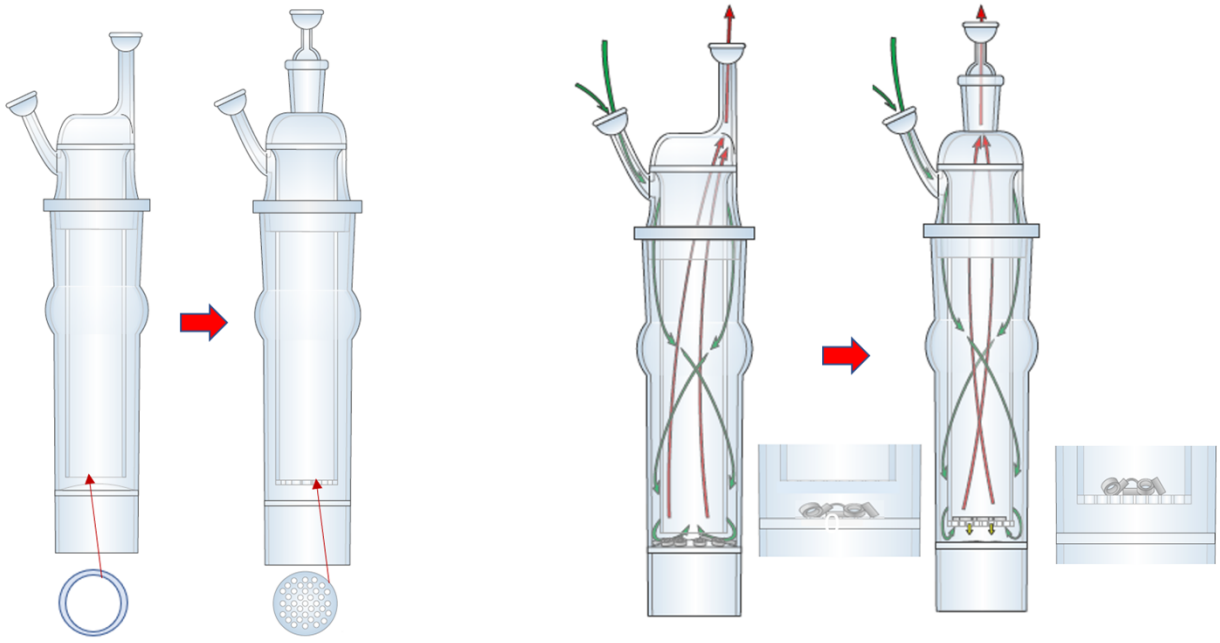

Chimney as an open tube vs. staged chimney W rings sit on bottom vs. on the stage

Figure 28. Vessel chimney structure change with W rings on perforated stage instead of vessel bottom.

The major change to the quartz reaction vessel is the chimney, which was revised from a straight open tube to one with a perforated stage for the W rings or pellets sit on instead of on the bottom of the vessel. The holes of the stage are 4 mm in diameter to ensure rings or pellets stay on stage, but WO_3 powder may

fall through the holes onto the vessel bottom. Previously when rings sit on vessel bottom, the large volume of converted WO_3 will cover the surface of W metal (Figure 9) while the air flow comes down from the jacket clearance (green arrow) bypassing rings into the chimney (red arrow) toward the off-gas exit. When metal rings sit on the stage, air flow squeezes into chimney through 4 mm holes and contacts W metal first by pushing WO_3 powder of lower density away (which falls to the vessel bottom or moves up). Because of better interaction of O_2 with W metal surface, W/O_2 reaction efficiency is expected to be enhanced.

3.3.2 Phase 3a: Heating pressed W–Os metal pellets in 750°C with an air flow of 1 L/min

The Phase 3a experiment was done by heating the W–Os metal pellets at 750°C in an air flow of 1 L/min, allowing W conversion to WO_3 with coproduced volatile OsO_4 being carried into NaOH traps by air flow. The analysis results of Os distribution will confirm the Os scrubbing effectiveness in Phase 2 experiment, and the W → WO_3 process will display the effect of new quartz vessel for conversion efficiency.

Eight W–Os pellets were loaded from a vial into the quartz chimney via the top joint opening (different from loading pellets into quartz vessel of original design) by tilting the vessel assembly to a proper angle. Next, W–Os pellets were gently guided onto the perforated bottom of the quartz chimney and arranged evenly on the perforated chimney stage with gentle shaking. The quartz assembly was placed into the furnace and connected with joint adaptor and a top glass L tubing. A thermal sensor was installed 2 in. above the glass ball joint along the glass L tube for temperature measurements at that spot, which was set up to have the temperature change with air flow rates, displayed in Figure 14. A mirror was installed above the vertical furnace to observe the inside of the reaction vessel (Figure 29).

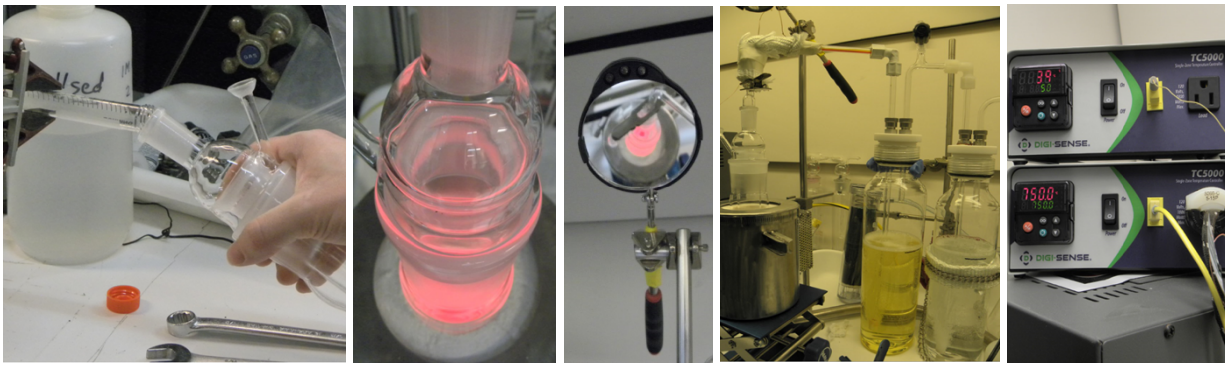

Figure 29. Pellet loading, heat control, and temperature measurements during the Phase 2 experiment.

The system was started in the following order. First, the vacuum pump was turned on, and the air flow was regulated to 1 L/min using a digital flow meter. Next, the heating controller was turned on, and the temperature was increased in 100°C increments until the final operating temperature of 750°C was reached. Once the furnace was turned on, the temperature of the furnace and the glass L tube 2 in. above the ball joint were measured and recorded using thermocouples.

It took 77 min for the furnace to heat from room temperature to 750°C at an air flow of 1 L/min and for the 2 in. spot to reach 38°C. The heating was continued at 750°C and an air flow of 1 L/min for an additional 60 min, while 2 in. spot reached 40°C. The air flow was then adjusted to 2 L/min but maintained furnace temperature of 750°C for another 14 min, while the 2 in. spot temperature reached 85°C. To cool the system, the heating was stopped while the air flow continued. The total heating time at 750°C in this run was 74 min. The trial of temperature measurements at 2 in. spot with varying air flow was started immediately but stopped after reaching an air flow of 2 L/min because the digital flow meter

malfunctioned. The same trial with an air flow up to 7 L/min was rerun later when heating unconverted W residual from W–Os pellets.

During heating at 750°C with air flow from quartz reaction vessel, invisible OsO_4 formed inside the vessel and was carried by air flow from the vessel into NaOH scrubbers. With the increased temperature, a dark zone was observed at the top part of vessel (outside the furnace). During heating at 750°C, this dark zone faded and some residual iodine species (possibly left from the Phase 2 experiment) inside the glass L tube liquidized, solidified, and then vaporized. The vapor was carried into the NaOH scrubber and formed the lighter (but typical) orange color of iodine species in NaOH liquid sorbent. As in Phase 2 work, samples from these two NaOH scrubbers were analyzed by ICP-OES for Os content of III-T-1 and III-T-2 vs. the Os input.

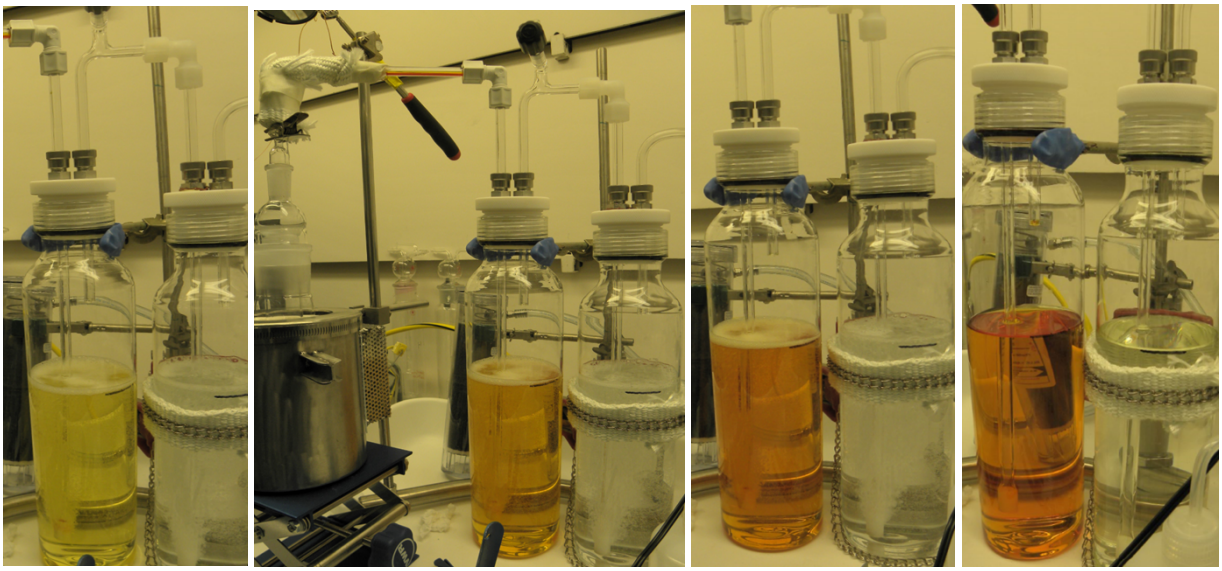

Figure 30. During 74 min color changes of NaOH traps due to OsO_4 and I_2 absorption.

After completely cooling, the vacuum pump was turned off (after the negative pressure released via the relief valve). The quartz vessel was pulled out of furnace for inspection. It was observed that green WO_3 powder, more than 10 times of the volume of that of the pellets, piled up on top of the perforated stage inside the chimney (only small amount of WO_3 powder fell onto the bottom of quartz vessel). Most of the powder fell through the holes into the vessel bottom by shaking. A known volume of 6 *M* NaOH was used to wash the residue powder into the vessel. The slurry of WO_3 powder/NaOH was later transferred into a glass jar and was left sitting without stirring and warming for further dissolution. It took about 76 hours to dissolve the WO_3 powder, leaving a trace of unknown solid black fines, which was weighed 10 mg in a filter with 0.2 µm paper (1.6 µm paper failed to catch the fines previously). This 72.5 mL of dissolved W (in tungstate form) solution is named as III-G-1 solution.

After air drying, the undissolved W chunks (Figure 31) were weighed at 0.1305 g (3.28% of total input W 3.9784 g), and then loaded back into the quartz vessel. The furnace/vessel was again connected through the glass L tube to a single scrubber of 1 L of 1 *M* NaOH, followed with knock out flask, charcoal canister and a digital flowmeter to the vacuum pump. The residual W chunks were heated (after being soaked in 6 *M* NaOH) up to 750°C at an air flow of 1 L/min. The temperature at the 2 in. spot above the glass joint was measured, and then the furnace temperature was increased once the temperature at the 2 in. spot reached steady state (Figure 14). After the air flow was increased to 7 L/min and maintained for about 15 min, the temperature reading for 2 in. spot reached 243°C (Section 3.1.3). In this process, the residual W chunks were heated at 750°C in varying air flow rates for a total 138 min. After system

cooled, the residual chunks showed no obvious changes. The 1 L of 1 *M* NaOH in scrubber was collected as solution III-G-02 for Os content analysis.

Pre-/after shaking WO_3 washed into a jar WO_3 dissolved in 6 *M* NaOH

Figure 31. W pellets converted to WO_3 powder at 750°C and then dissolved into 6 *M* NaOH.

The chunks were soaked in 5 mL of 30% H_2O_2 for dissolution of residual unconverted W metal [7]. The chunks collapsed into powder after soaking in H_2O_2 for 7 hours but showed no additional changes after additional soaking. After 101 hours in H_2O_2, the solution was filtered with a 0.2 μm paper. The remaining solids weighed as 0.0631 g (i.e., 0.0674 g of solid was possibly dissolved as W metal by H_2O_2).

The entire trial led to the following conclusions about the W metal portion of the eight pellets:

1. With better interactions of O_2/W, W→WO_3 conversion reached an apparent rate of 96.47% of the W metal input [3.9784 – (0.1305 + 0.010 black fines)/3.9784], within 74 min at a low air flow of 1 L/min.

2. Once the residual chunks had been soaked in 6 *M* NaOH, extended heating at 750°C at varying air flows in the furnace will not achieve further W→WO_3 conversion (smashing the chunks before heating may improve this), although later ICP-OES analysis of III-G-02 solution showed that about 9.1 mg of Os was converted into OsO_4 and absorbed by 1 L of 1 *M* NaOH trap (see Table 5).

3. Some of the residual chunks (without being smashed) can be dissolved using H_2O_2, but they might be unconverted W metal after heating at 750°C twice. The chunks undissolved in H_2O_2 was weighed as 0.0674 g after filtration and drying. If deducting the weight of 9.1 mg Os (in III-G-02) from 0.1305 g, there was only 44.5% of heating residual being dissolved in H_2O_2 [(0.1214 – 0.0674)/0.1214].

Now, the behavior of Os metal portion in the eight W–Os pellets will be evaluated during heating and scrubbing operations, focusing on Os distribution along the scrubbing array (i.e., Os content in two NaOH traps [III-T-1 and III-T-2]) and the remains inside the quartz reaction vessel after 74 min heating at 750°C and air flow of 1 L/min. As described earlier, the dissolved remains in the quartz vessel include solution

from III-G-01 and III-G-02. If assuming the undissolved 0.0674 g solids are undissolved Os remains (the part dissolved by H_2O_2 is not considered an Os compound), the total Os remains in quartz reaction vessel would be the sum of Os in III-T-1, III-T-2, and 0.0674 g solids.

The distribution of Os portion of eight pellets is displayed in the Table 5, where the subtotal Os mass was a sum of the average duplicates of all sample results plus 67.4 mg, although the second result of the duplicates of III-T-1 was claimed as too high due to the "memory effect" of the ICP-OES instrument.

Table 5. Calculation sheet based on the first ICP-OES analysis of Phase 3a samples.

1/28/2021	**Tot Os(mg)**	946.92	Tot W (mg)	3978.48	Tot pellets	4925.4				
	1st Analytical Data for Phase-3a run									
	0.94692	g			ICP-OES Analyzed results per 4 emission peaks (ug/mL)					
1st ICP-OES		**Os (mg)**	**Tot-V mL**	**Ave ug/mL**	**S-mL**	**228nm**	**207nm**	**219nm**	**226nm**	
	III-T-1	814.69838	1500	**543.1323**	5	547.204	547.762	544.445	533.118	
	III-T-1	916.11713	1500	**610.7448**	5	616.35	614.449	611.309	600.871	
	III-T-2	2.029	1500	**1.352667**	5	1.34	1.379	1.339	1.32	
	III-T-2	2.137	1500	**1.424667**	5	1.438	1.441	1.395	1.379	
	III-G-1	5.0203531	72.5	**69.24625**	5	251.58	17.603	0	7.802	
	III-G-1	4.9845381	72.5	**68.75225**	5	249.858	17.497	0	7.654	
	III-G-2	9.0456667	1000	**9.045667**	5	9.132	8.894	9.111	8.916	
	III-G-2	9.1765	1000	**9.1765**	5	9.402	9.05	9.221	9.033	
				0	5	0	0	0	0	
			% vs Total	**0**	5	0	0	0	0	
6M NaOH	Undisslved	140.5	0.028526	(130.5 mg chunks + 10 mg black fines)						
H2O2	Undisslved	67.4		(130.5 mg chunks - 63.1 mg in H2O2)				Assum dissolved 63.1 mg as W metal.		
	sub-t-Os	898.2949	**0.948649**	94.86492	%	**Question:**	Will mass of undissolved by H2O2 be part of Os?			
							Will mass of the black fines be part of Os?			

To confirm the first set of analytical results, a second batch of the samples III-T-1 and III-T-2 was analyzed again in triplicate with ICP-OES. The new results of III-T-1 and III-T-2 replace the first batch sample data and are displayed in Table 6.

Table 6. Calculation sheet based on the second ICP-OES analysis of Phase 3a samples.

2/15/2021	Tot Os(mg)	946.92	Tot W (mg)	3978.48	Total	4925.4				
	2nd Analytical Data for Phase-3a run									
	0.94692				ICP-OES Analyzed results per 4 emission peaks (ug/mL)					
1st ICP-OES		Os (mg)	Tot-V mL	Ave ug/mL	S-mL	228nm	207nm	219nm	226nm	
	III-T-1	*791.366625*	*1500*	***527.578***	*5*	*520.789*	*528.899*	*525.697*	*534.926*	
	III-T-1	*803.53275*	*1500*	***535.689***	*5*	*526.994*	*537.866*	*534.305*	*543.589*	
	III-T-1	*810.195*	*1500*	***540.13***	*5*	*531.223*	*541.996*	*538.421*	*548.88*	
	III-T-2	*2.488*	*1500*	***1.65867***	*5*	*1.621*	*1.726*	*1.629*	*1.683*	
	III-T-2	*2.4135*	*1500*	***1.609***	*5*	*1.575*	*1.671*	*1.581*	*1.644*	
	III-T-2	*2.396*	*1500*	***1.59733***	*5*	*1.565*	*1.659*	*1.568*	*1.628*	
from 1/28	III-G-1	5.02035313	72.5	**69.24625**	5	251.58	17.603	0	7.802	
from 1/28	III-G-1	4.98453813	72.5	**68.75225**	5	249.858	17.497	0	7.654	
from 1/28	III-G-2	9.04566667	1000	**9.045667**	5	9.132	8.894	9.111	8.916	
from 1/28	III-G-2	9.1765	1000	**9.1765**	5	9.402	9.05	9.221	9.033	
				0	5	0	0	0	0	
			% vs Total	**0**	5	0	0	0	0	
6M NaOH	Undisslved	140.5	0.028526	(130.5 mg chunks + 10 mg black fines)						
H2O2	Undisslved	67.4		(130.5 mg chunks - 63.1 mg in H2O2)			Assum dissolved 63.1 mg as W metal			
	sub-t-Os	885.644154	**0.935289**	93.52893	%	**Question:**	Will mass of black fines be part of Os?			

The triplicates of III-T-1 results confirmed that among the first duplicated data, the highlighted number was a data point influenced by a positive interference. The results indicating that 800 mg of Os in Trap 1 are reliable based on the two sets of ICP-OES analysis.

In addition to W/WO_3 conversion efficiency, the capability of the OsO_4 scrubbing system is our top concern.

Table 7. Osmium distribution pattern along the OsO_4 generating and scrubbing system.

Phase-3a							
Os, %	**G-1 73.5mL**	**G-2, 1L**	**Solids**	**Trap-1 1.5L**	**Trap-2 1.5L**		**Total mg**
Data #1	5.00245	9.1111	67.4	814.7	2.06	mg	898.2736
	0.00556896	0.0101429	0.075033	0.906962	0.0022933	(x100%)	
		0.0907447	(x100%)	0.998888	0.0025222	(x100%)	
Data #2	5.00245	9.1111	67.4	801.7	2.4325	mg	885.6461
	0.00564836	0.0102875	0.076103	0.9052149	0.0027466	(x100%)	
		0.0920385	(x100%)	0.9988722	0.003025	(x100%)	

One conclusion is obvious: there is no volatile OsO_4 breakthrough in the newly designed scrubbing array. Many times more OsO_4 was generated than that from a fully loaded target of 4.833 g W metal during a normal campaign. This does not count possible OsO_4 deposits on top part of quartz vessel or deposits on the L tube that were not leached or sampled into input Os mass balance. The sum of three major parts of Os (OsO_4 generator, and two traps) in Phase 3a are 94–95% of the Os amount originally put into the quartz vessel. High recovery rates of Os support the reliability of the two sets of analytical data. As to the question of if the 67.4 mg of solids should be counted as Os or not, we noticed that the total absorbed Os

in two traps is 99.9% in Trap 1 with only 0.25–0.3% in Trap 2. The data of 2 mg Os in Trap 2 (1.5 L) is a roundup number from small sample and possibly reflects a detection limit.

There is no sign of an Os saturation in Trap 1 with 800 mg of Os trapped, since in Phase 2 experiment the Trap 1 absorbed not just comparable amount Os (vs. in Phase 3a) but also >6 times of iodine species in the Trap 1 without carry over to Trap 2 (judged by the colors in Trap 1 and 2). Let's assume 800 mg of Os has already saturated one stage of NaOH trap, then further assume that the two 1.5 L 1 *M* NaOH traps would absorb at least 1.6 g of Os (8.377 mmole if as $^{191}OsO_4$). This trapped 1.6 g of Os by two NaOH traps is already (1.6/0.5=) 3.2 times of the "most conservative maximum of Os" (0.5 g) to be generated in a normal (4.833 g W, 40 days cooling) ^{188}W process.

The most conservative amount of Os determined by the ISOCHAIN (default) model uses an incorrect ^{187}W neutron absorption cross section and does not count the significant neutron flux attenuation inside W metal target. Irradiation modeling scientists considered the MCNP6-ORIGEN model (the red curve in Figure 16), which is closer to the campaigns. The total Os amount calculated for a normal campaign (4.833 g W, 40 days cooling) per MCNP6-ORIGEN model is 166 mg of Os (0.87 mmole as in $^{191}OsO_4$ form), with which the 1.6 g of NaOH trapped Os is already 9.64 times of Os to be generated in a normal campaign process. Once counting on solid sorbents contributions to OsO_4 retention, it is safe to say that the renovated OsO_4 scrubbing array is capable of absorbing 10 times of OsO_4 generated in a normal ^{188}W process.

The results from Phase 3a experiment proves the effectiveness of new scrubbing array and the tentative conclusion from Phase 2 experiment. Further, Phase 3a demonstrated the improved W/WO_3 conversion using the quartz reaction vessel with the new design, although the efficiency of converting a sintered W metal target into WO_3 would be arguably more difficult than simply using pressed W–Os metal pellets because the latter have a higher surface area and porous defects due to Os evaporation in heating. Consequently, a Phase 3b experiment was performed with eight sintered natural W metal rings.

3.3.3 Phase 3b: Heating sintered W metal rings in 750°C with an air flow of 1 L/min

This Phase 3b experiment carried out a similar process as in Phase 3a, but eight sintered W metal rings were heated instead of the pressed W–Os metal pellets. Since no volatile Os involved, the scrubbing system employed the same array but with only one NaOH scrubber of 1 L 1 *M* NaOH.

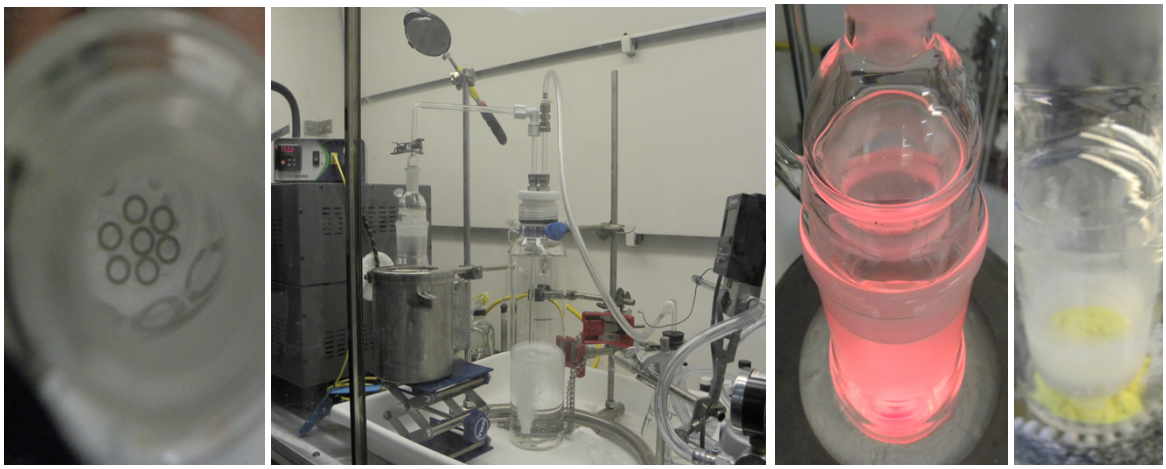

Figure 32. Tungsten rings in the chimney, with controlled heating/scrubbing in Phase 3b experiment.

With knowledge of >96% W/WO_3 conversion efficiency by 750°C in only 74 min in Phase 3a run, a 3 hour 750°C heating in an air flow of 1 L/min was determined before starting work, which considers the robustness of sintered natural W metal rings.

Eight sintered W rings were loaded from a vial into the quartz chimney in the same manner as in Phase 3a. Eight W rings were gently guided onto the perforated bottom of the quartz chimney and arranged evenly on the perforated chimney stage with gentle shaking. The quartz assembly was placed into the furnace and connected with joint adaptor and a top glass L tubing, but this time the thermal sensor was installed for measurements above furnace temperature, as was done in 3a.

The system was started in the same order as in 3a. The vacuum pump was turned on, and the air flow was regulated to 1 L/min using a digital flow meter. Then the heating controller was turned on to increase the furnace temperature stagewise to 750°C in 49 min. A temperature of 750°C and air flow of 1 L/min were maintained for 3 hours (180 min), and then the heating was stopped for cooling with the air flow on.

After the furnace cooled, the vacuum pump was stopped (no need for negative pressure release because only one stage of the NaOH trap was used). The quartz vessel was pulled out of furnace for inspection. The quartz chimney was no longer transparent after NaOH etching in Phase 3a run, but yellow WO_3 powder (not green), of more than 10 times of the volume than that of W rings, piled up on top of the perforated stage inside the chimney. Only some of powder fell onto the bottom of quartz vessel. Most of the powder was shaken through the holes into the vessel bottom, leaving a couple of loose chunks stuck at holes of the stage. A known volume of 6 *M* NaOH was used to wash the powder into the vessel (the loose chunks fell to the vessel bottom in a few hours). The powder was later transferred into a glass jar and left to sit to dissolve without stirring and warming up.

The WO_3 powder was gradually dissolved into 6 *M* NaOH, changing in color from yellow to green to olive (mixed with grey/black chunks). Only some visible powder and solid chunks remained (Figure 33). Above dissolution process took 96 hours before the glass jar was sealed into a plastic bag and kept in a water bath of 55°C. The visible powder was dissolved after 2 hours at 55°C in 6 *M* NaOH, leaving solid chunks only in 6 *M* NaOH solution. 24 more hours at 55°C in 6 *M* NaOH didn't dissolve the remaining grey/black chunks (looked like unconverted W metal residue). Dissolution in 6 *M* NaOH was stopped.

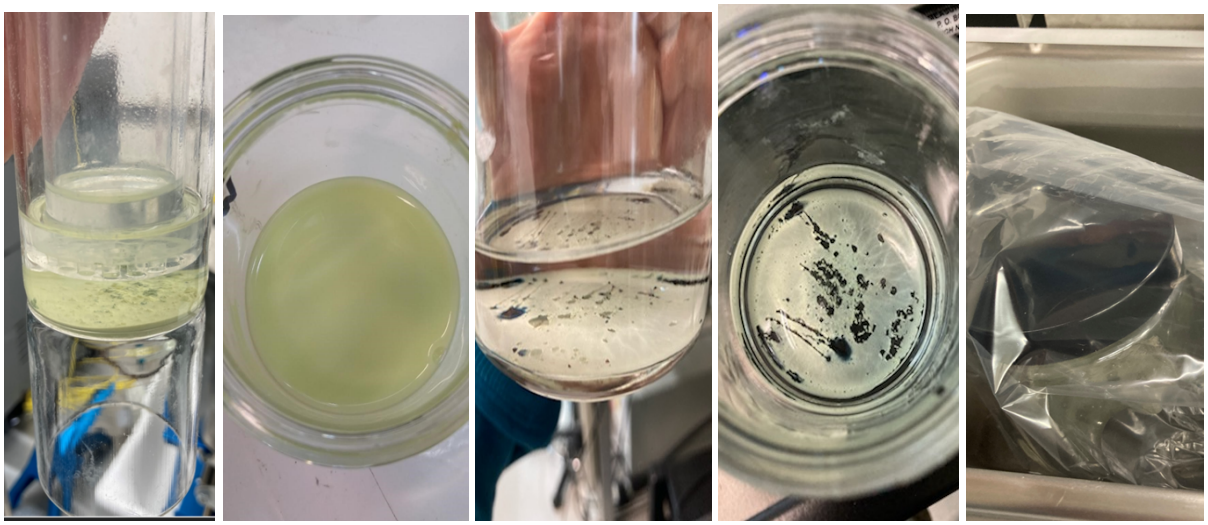

Figure 33. Phase 3b: dissolution of WO_3 in 6 *M* NaOH at room temperature for 96 hours.

The 6 *M* NaOH solution was filtered with 1.6 μm paper, and the undissolved grey/black chunks weighed 0.1223 g (Figure 34). These chunks were poured into 5 mL of 30% H_2O_2 with no shaking or warming. They were completely dissolved by H_2O_2 in 19.5 hours.

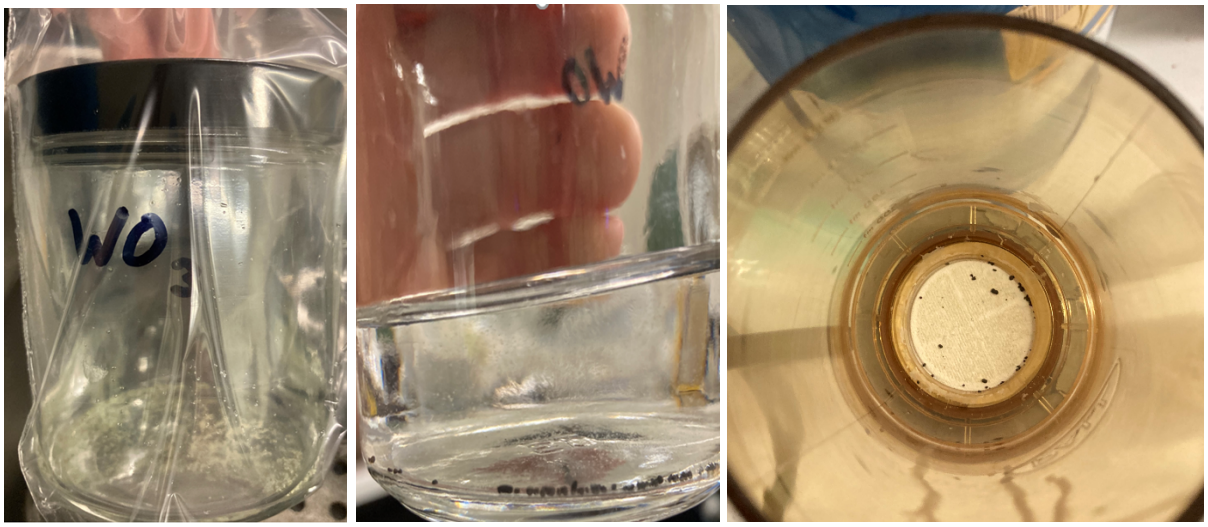

Figure 34. After additional 26 hours of WO_3 dissolution in 6 *M* NaOH at 55°C.

If this 0.1223 g of solid material was considered as insoluble in 6 *M* NaOH, the dissolvable WO_3 (took more effort to dissolve than WO_3 in 3a) would weigh (4.8904 – 0.1223 =) 4.7681 g (as in form of W metal), giving a W/WO_3 conversion rate of (4.7681/4.8904 × 100% =) 97.50%, which is a slightly higher than the 96.47% in Phase 3a experiment.

	750°C	**Powder color**	**W/WO_3 conversion**	**NaOH, room temperature**	**NaOH, 55°C**
III-3a	74 min	Yellowish green	96.47%	76 hours	0
III-3b	180 min	Greenish yellow	97.50%	96 hours	2 hours or more

In terms of W/WO_3 conversion, the difference of the results from Phase 3a and 3b is not obvious. There is not a clear explanation for the color difference of the converted WO_3 after 74 min or 180 min heating at 750°C, or why it behaved so differently in dissolution of 6 *M* NaOH at room temperature. Fortunately, both should be easily dissolved in 6 *M* NaOH at 55°C, and the campaign practice of WO_3 dissolution in 6 *M* NaOH has always been performed at a warm-up temperature.

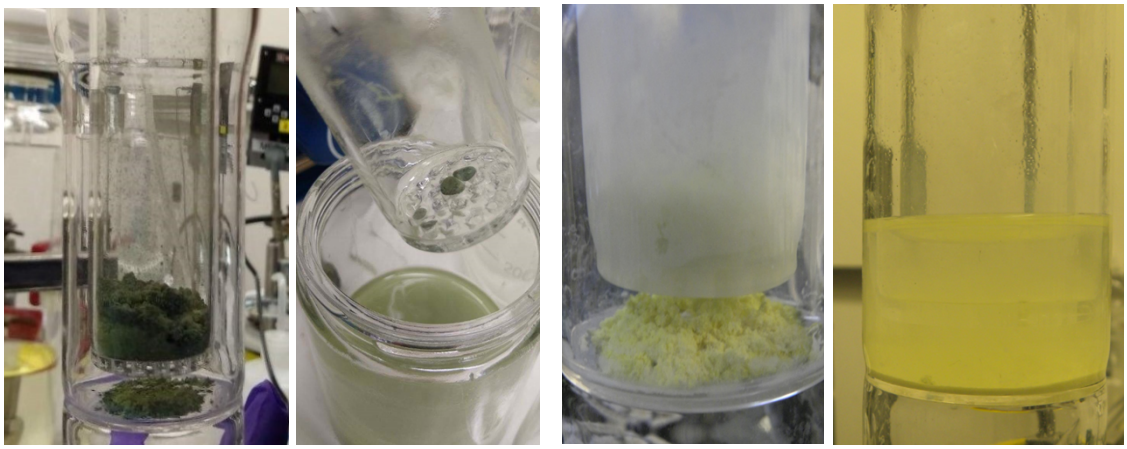

Figure 35. Color difference of WO_3 in 3a and 3b and their dissolution in 6 *M* NaOH.

The color of WO_3 is commonly addressed as yellow in W industry, but green WO_3 was not uncommonly seen, which was referred as nonstoichiometric tungsten oxides due to loss of oxygen [8]. In this work, the W conversion to WO_3 or $WO_{<3}$ is of no concern, as long as the W is soluble in 6 *M* NaOH for ^{188}W recovery. More important is that a soluble tungsten oxide can be obtained in a reasonably short heating period with a high conversion efficiency. Experimental results show that extended heating times may not achieve a dramatic increase in the W/WO_3 rate, so the new operation procedure defines a maximum of 4 hours of heating at 750°C as a control parameter in future ^{188}W campaigns.

3.4 DIRECTIONS FOR FUTURE STUDIES

3.4.1 Recovering ^{188}W with zero possibility of ^{191}Os release

Current heterogeneous conversion method to treat the irradiated ^{186}W metal target achieves two goals simultaneously. First, it converts the product ^{188}W metal into a soluble form and, second, it separates the by-product ^{191}Os in a volatile form away from the ^{188}W that would then need to be absorbed by subsequent sorbent scrubbing. However, the generation/existence of volatile OsO_4 during heating means that it is possible OsO_4 could be released if the scrubbing array malfunctions or if mistakes were made in array arrangement or during operations. The incident of minor amount of ^{191}Os release in July 2020 in Building 4501 was a single example of such case.

Generation of ^{191}Os cannot be avoided during production of ^{188}W. But can we avoid generation of volatile OsO_4, the root cause of ^{191}Os release? To accomplish this, heating the irradiated W metal target must be avoided to prevent the oxidation reactions in Eqs. 1 to 3. The alternative is to directly dissolve the W metal target using a selected reagent that dissolves the W metal selectively but leaves Os undissolved in solid form. Solid Os in dissolved W solution could be filtered away from the ^{188}W product without creating volatile $^{191}OsO_4$, eliminating the possibility of release of ^{191}Os into environment! The key point of this process direction is to find such a reagent to achieve a selective dissolution of W metal followed with solid Os removal.

3.4.2 Further studies on method of generating OsO_4 by reacting Os metal with $NaIO_4$

As described in Section 3.2.3, mixing Os metal powder with $NaIO_4$ in DI water while stirring and air purging will generate volatile OsO_4, which has been proven by the presence of reduced solid product OsO_2 in organic NPH layer. But questions remain: Is the assumed reaction Eq. 7 correct or not? With excessive amount of $NaIO_4$ added in Phase 2 experiment, how did the excessive I^- and IO_4^- become a volatile I species and transfer into NaOH traps with relatively low air purging (50–70 mL/min), forming a

dark orange color that is typical of iodine-NaOH compounds? Since a higher percentage of Os remained in the OsO_4 generator, what will be the maximum percentage yield by this wet method for OsO_4 generation vs. input Os metal powder in the generator?

As indicated, this method of OsO_4 generation has an advantage of not carrying acid to caustic traps and as an alternative pathway of OsO_4 generation; consequently, it deserves further attention to resolve the questions above.

3.4.3 Analysis improvement of Os content in liquid samples containing iodine species

As mentioned in Section 3.2.3, Os content analysis for samples from Phase 2 work (I species involved due to OsO_4 generating method of reaction of Os with $NaIO_4$) by ICP-OES or ICP-MS encountered a positive interference with Os samples containing I species. A calibration curve of iodide would not reduce the positive interference (the interference of iodine species not in form of iodide). Changing the sample order and adding extensive rinses between each sample improved the analysis of some of the samples, including II-T1, but this was not true for the II-G1 sample with extremely high iodine content. Our efforts with UV-Vis spectroscopy analysis of these samples mitigated the positive interference but without a precise calibration of iodine species. Exploring a chemical separation method for a quick removal of either Os or I in such samples would make the above-mentioned studies of aqueous OsO_4 generation by Os metal and $NaIO_4$ more efficient and practical.

3.4.4 Studies of solid sorbents and other liquid sorbents for volatile OsO4 scrubbing

Liquid sorbents of volatile OsO_4 have been used as major sorbents in OsO_4 scrubbing systems, especially NaOH, because of its high loading capacity to OsO_4 [9]. Other liquid sorbents, such as NPH, have a high loading capacity to volatile OsO_4, plus it has a high selectivity to tetra oxides (no absorption to iodine species). However, considering organic liquid waste disposal, NPH would not be the first choice for OsO_4 scrubbing. But the reduced Os product in NPH phase, solid OsO_2, can be separated by filtration to allow NPH to be reused when Os become a byproduct for recovery.

The interaction efficiency of gas/solid reactants is lower than that of gas/liquid reactants when the reactant in gas phase is the major concern. Lack of the knowledge about the OsO_4 loading capacity for these solid sorbents (e.g., Tygon tubing or charcoal) meant they were only used as supplementary sorbents in the OsO_4 scrubbing process. The fact that OsO_4 can be absorbed by Tygon tubing is well known to ^{188}W process operators who had observed tubing color changes as OsO_4 passed through.

Future nonradiological OsO_4 experiments with Tygon tubing of different brands and other sorbent materials should determine their OsO_4 loading capacities and loading mechanisms, which would greatly help design the perfect scrubbing system.

3.4.5 Resolving the puzzle of different colors of WO_3 from conversion of different batches

The color difference of the converted WO_3 in Phase 3a vs. Phase 3b remains a puzzle. We saw pictures of green or yellow WO_3 in several resources, although WO_3's color is commonly described as yellow. Differences between the W metal used in the two experiments are listed here:

W batch no.	W metal particles	Sources	Shape, preheating	Sintering (argon)	Time under 700°C (air)	Resulting WO_3 color	W/WO_3
Phase 3a	10 μm, 99.99%	Alfa Aesar	Pressed W–Os pellets	N/A	74 min	Yellowish green	96.47%

Phase 3b	8–12 µm, 99.9%	Alfa Product (1970s)	Pressed W rings	1,400°C, 4 hours	180 min	Greenish yellow	97.50%

The literature [8] refers to the green color of WO_3 powder as *nonstoichiometric tungsten oxides* due to loss of oxygen. In our experience with W/WO_3 conversion, we would like to refer this as the result of incomplete oxidation instead, if the green color was due to $WO_{<3}$. The green product was obtained in a shorter heating time of 74 min, which seems to support this assumption. For our WO_3 dissolution needs, the converted product needs to be soluble in 6 *M* NaOH at this step, no matter whether it is $WO_{<3}$ or WO_3. In our two Phase 3 runs, the dissolution rates of the solids were fairly close, despite the different heating periods. Dissolution in 6 *M* NaOH under room temperature showed the dissolution of green product even easier than yellow product. But we are not sure that shorter heating period would certainly have the WO_3 powder easier in dissolution of 6 *M* NaOH. Obviously, extended tests are needed for confirmation.

4. CONCLUSION

Revisions have been made to ^{188}W process of 2006 to enhance the two major heterogeneous reactions of $W\text{-}WO_3$ conversion and OsO_4 absorption by NaOH, based on three phases of experiments.

With results from Phase 1 experiments, specific air flow limits were determined for both the redesigned scrubbing array and the current scrubbing array at Building 4501. The excessively high air flow used in previous campaigns has been recognized as the root cause of the failure of the NaOH scrubber in previous campaigns and as a cause of a possible heating damage to the Tygon tubing connected near furnace.

Results from both the Phase 2 and Phase 3a runs proved the new design of the OsO_4 scrubbing array is capable of absorbing 10 times of OsO_4 generated in a normal ^{188}W process. The key parameters of air bubble size (decided by frit size) and their travel distance in NaOH (determined by length of air inlet tube merged in NaOH) in the design of the NaOH scrubber are emphasized. The maximum air flow in ^{188}W process was determined to be ≤2 L/min.

Both the Phase 3a and 3b runs proved the redesigned quartz reaction vessel enhanced the conversion efficiency of W → WO_3 from heating at 750°C for days down to only 3 hours at 1 L/min (vs. previous at 7 L/min or higher). The key design change is the inside chimney structure, which now allows better interaction of air (O_2) with the W metal surface. The improvements of OsO_4 scrubbing array and the reaction vessel were aimed at enhancing the two major heterogeneous reactions in ^{188}W process, and they are effective in tests with non-rad targets of W and Os. In terms of efficiency enhancement of the two major heterogeneous reactions, the preset goals of ^{191}Os mitigation and more efficient W → WO_3 conversion have been successfully reached.

The revisions made so far cannot prevent all potential problems. For example, in the High Flux Isotope Reactor the W metal rings are irradiated for two cycles (45 days total) with an in-rabbit temperature as high as 1,180°C, which is effectively a 2nd –long term—sintering step. This is in addition to the sintering of only 4 h at 1,400°C prior to irradiation. This could result in changes of W metal rings' metallurgic structure or formation of W alloys with Re (decay daughter) or carbon (residue from pellet pressing lubricant) may occur. Either case would possibly retard the W to WO_3 conversion in the ^{188}W process. Further studies on improving the W to WO_3 conversion and OsO_4 scrubbing should be continued. To guarantee there is zero opportunity for an $^{191}OsO_4$ release, a new pathway for selective dissolution of irradiated W metal target should be studied with the goal of W dissolution but no generation of volatile OsO_4 in the process.

5. REFERENCES

1. S. Mirzadeh, M. Du, A. Beets, and F. F. Knapp Jr., "Thermoseparation of Neutron-Irradiated Tungsten from Re and Os," *Ind. Eng. Chem. Res.*, 39, 3169–3172, 2000.
2. "Processing of HFIR-Irradiated Tungsten-186 Targets" Procedure MRP-W-188-001.0, Oak Ridge National Laboratory, Oak Ridge, TN, approved on July 6, 2015 (Supersedes the Procedure NMP-cGMP-W-188-007B.1)
3. J. R. Griswold et al., Theoretical Yields for ^{188}W Production in the High Flux Isotope Reactor, ORNL/TM-2020/1859, Oak Ridge National Laboratory, Oak Ridge, TN, 2021.
4. S. H. Bruffey and B. B. Spencer, "Characterization of Ruthenium Tetroxide Capture from Dry Gas Streams by Silica Gel and Metal Surfaces." *Proceedings of Global 2019*, September 2019.
5. T. E. Geswindt, W. J. Gerber, H. E. Rohwer and K. R. Koch, "A Kinetic and Thermodynamic Study of the Unexpected Comproportionation Reaction between cis-$[OsVIIIO_4(OH)_2]^{2-}$ and trans-$[OsVIO_2(OH)_4]^{2-}$ to form a Postulated $[OsVIIO_3(OH)_3]^{2-}$ Complex Anion," Dalton Transactions, 40, 8581, 2011.
6. M. Du, "Confirmative Non-Rad Test for Recovery of ^{106}Ru," presented at the Isotope and Fuel Cycle Technology Division Seminar Series, Oak Ridge National Laboratory, Oak Ridge, TN, February 19, 2020.
7. Peter C. Murau, "Dissolution of Tungsten by Hydrogen Peroxide," *Analytical Chemistry*, 33(8), 1125–1126, July 1961.
8. Matthias Weil and Wolf-Dieter Schubert, "The Beautiful Colors of Tungsten Oxides," *Tungsten Newsletter*, June 2013 P1-4, ITIA.
9. Alexander Illis and Alan Manson, "Method for Production of High Purity Osmium," US Patent 3,536,479, October 27, 1970.